1	Human Activities Caused Hypoxia Expansion in a Large Eutrophic
2	Estuary: Non-negligible Role of Riverine Suspended Sediments
3	
4	Yue Nan ¹ , Zheng Chen ² , Bin Wang ³ , Bo Liang ⁴ , Jiatang Hu ^{1,5,6*}
5	
6	¹ School of Environmental Science and Engineering, Sun Yat-Sen University,
7	Guangzhou, 510275, China
8	² Earth, Ocean and Atmospheric Sciences Thrust, The Hong Kong University of
9	Science and Technology (Guangzhou), Guangzhou, 511455, China
10	³ Department of Oceanography, Dalhousie University, Halifax, Nova Scotia, Canada
11	⁴ Eco-Environmental Monitoring and Research Center, Pearl River Valley and South
12	China Sea Ecology and Environment Administration, Ministry of Ecology and
13	Environment of the People's Republic of China, Guangzhou, 510611, China
14	⁵ Guangdong Provincial Key Laboratory of Environmental Pollution Control and
15	Remediation Technology, Guangzhou, 510275, China
16	⁶ Southern Marine Science and Engineering Guangdong Laboratory (Zhuhai), Zhuhai
17	519000, China
18	
19	Correspondence: Jiatang Hu (hujtang@mail.sysu.edu.cn)
20	

Abstract

21

22

23

24

25

26

27

28

29

30

31

32

33

34

35

36

37

38

39

40

41

42

43

44

45

46

47

48

Increase in riverine nutrient loads was generally recognized as the primary cause of coastal deoxygenation, whereas the role of other riverine factors, especially suspended sediments, has received less attention. This study aims to discern the impacts of anthropogenic alterations in various riverine inputs on the subsurface deoxygenation over the past three decades in a large river-dominated estuary, the Pearl River Estuary (PRE). Using aBy utilizing the physical-biogeochemical model, we reproduced the observed dissolved oxygen (DO) conditions off the PRE in the historical period (the 1990s with high_-suspended sediments_concentration (SSC), high_-DO, and low_nutrients inputs) and the present period (the 2010s with low-suspended sediments-DO SSC, low DO, and high_-nutrients_inputs).-In the 2010s, the PRE exhibited Due to the decadal changes in riverine inputs, the PRE has witnessed more extensive and persistent summer hypoxialow-oxygen events during summer in the 2020s, with the larger spatial extents of ~2926 km² for low oxygen area (DO < 4 mg/L,) increased expanding by \sim 148% (to \sim 2926 km²)relative to the 1990s) and 617 km² for the hypoxia area (DO < 3) mg/L) increasing, by 192% (to ~617 km²)) and longer duration (by ~15-35 days), evolving into three distinct hypoxic centers controlled by different factors. Low-oxygen durations extended to 15-35 days, and three distinct hypoxic centers formed under different controlling factors. Single-factor Model experiments suggested that the decreased riverine DO content (46%) alone- expanded low-oxygen areas in the upper estuarine regions by 44%, the decreased SSC (by 60%) alone cause a 47% expansion in the lower reach of PRE, and the increased nutrients alone (100% in dissolved inorganic nitrogen and 225% in phosphate) drove a 31% expansion has led to a lowoxygen expansion in the upper regions, accounting for 44% to the total increment. Meanwhile In comparison, the increased combined nutrient increases levels (100% in nitrogen and 225% in phosphorus) and the SSC declines declined suspended sediment concentration (60%) synergistically have jointly promoted enhanced the primary production and bottom oxygen consumptions (dominated by sediment oxygen uptake),

amplifyingthus resulting in a substantial enlargement of low-oxygen area (104%) and hypoxic-area (192%) area growth in the lower estuaries reaches. Our results revealed that SSC declines, by improving light availability for productivity, play a larger role than nutrient increases in exacerbating deoxygenation off the PRE. This synergy complicates hypoxia mitigation efforts focused solely on nutrient controls. Given the widespread global declines in riverine suspended sediments, our findings underscore the importance for incorporating sediment-mediated processes, a relatively overlooked factor, in coastal deoxygenation studies.a more critical role of the riverine suspended sediment decline than the nutrient increase in the exacerbation of eutrophication and deoxygenation off the PRE via improving light conditions to support higher local productivity, which could further amplify the effect combined with the growth in nutrients and confound the effectiveness of hypoxia mitigation under nutrient controls. Overall, in the context of global changes in riverine suspended sediments, it is imperative to reassess the contribution of riverine inputs to the coastal deoxygenation worldwide over the past decades, given that the impact of suspended sediments has been constantly overlooked in relevant investigations.

65 **Key words:** Deoxygenation; suspended sediments; nutrient inputs; decadal changes;

66 Pearl River Estuary

49

50

51

52

53

54

55

56

57

58

59

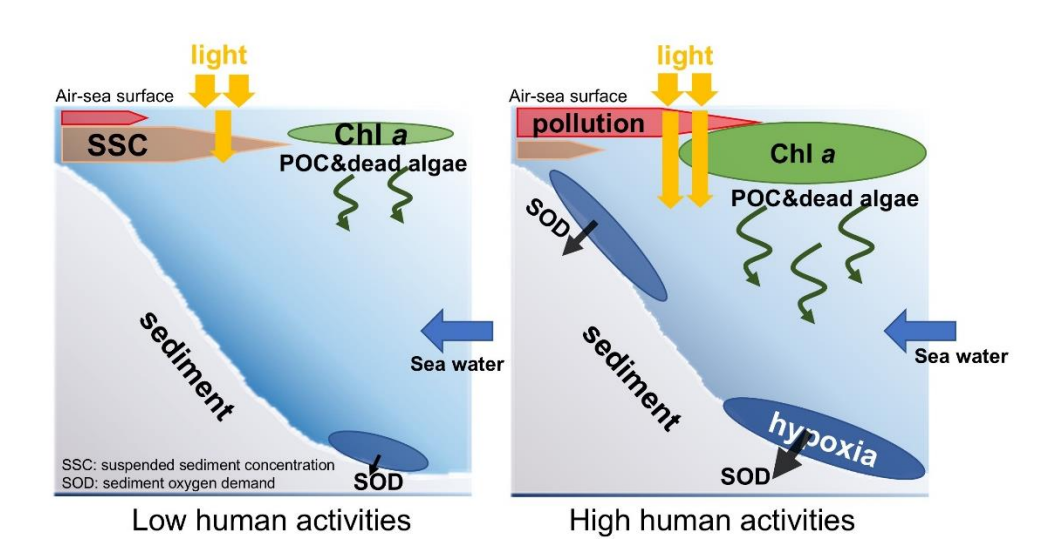
60

61

62

63

67 Graphical Abstract



1. Introduction

Hypoxia emerges when dissolved oxygen (DO) concentration drops below 3 mg/L in aquatic systems. It is an undesirable phenomenon which can lead to a series of biological and ecological consequences, such as damaging the habitat for aquatic organisms and imposing detrimental effects on the ecosystem community structure (Diaz and Rosenberg, 2008; Roman et al., 2019). Due to the substantial impacts from human socioeconomic activities, coastal regions have become a hotspot for hypoxia (Breitburg et al., 2018; Pitcher et al., 2021). Moreover, long-term exacerbation of hypoxia with spatial expansion and increased intensity-frequency has been frequently reported in estuarine and coastal regions worldwide during the past decades, including the Baltic Sea (Carstensen et al., 2014), the northern Gulf of Mexico (Bianchi et al., 2010), Chesapeake Bay (Murphy et al., 2011), the Yangtze River Estuary (Chen et al., 2017), and the Pearl River Estuary (Hu et al., 2021).

Plenty of studies were conducted to reveal the mechanism of hypoxia formation and evolution in coastal regions. It has been widely recognized that coastal deoxygenation is largely attributed to the eutrophication-driven production of organic

matters (Su et al., 2017; Wang et al., 2016; Howarth et al., 2011), which sink to the subsurface waters and bottom sediments, leading to intense oxygen depletion (Wang et al., 2014; Hagy et al., 2005). This would induce hypoxia when the density stratification restricts DO replenishment from the surface waters (Wang et al., 2018; Murphy et al., 2011). One important reason underlying eutrophication and hypoxia is the excessive nutrients that are discharged into the water column and stimulate phytoplankton blooms (Cullen, 2015; Wang et al., 2021; Cormier et al., 2023). In addition, Hhuman activities, such as dam construction (Bussi et al., 2021) and soil-water conservation measures (Yang et al., 2024) can significantly reduce suspended sediment in estuaries. - HenceIn addition, an improved light condition, e.g., due to the decreased suspended sediment loads, could also favor the enhancement of local production and hence hypoxia (Ge et al., 2020; Huang et al., 2022). The effects of nutrient and light conditions vary in coastal systems due to different hydrodynamic and topographic features, which makes the formulation of hypoxia mitigation strategies more challenging. Therefore, a quantitative assessment on the importance of these factors in generating hypoxia is crucial for understanding the primary drivers of hypoxia evolution and for proposing effective countermeasures.

A case in point is the Pearl River Estuary (PRE), which is situated in the northern South China Sea and close to the Guangdong-Hong Kong-Macao Great Bay Area (Fig. 1a). Owing to the relatively large nutrient inputs and vertical stratification formed by freshwater plume, hypoxia typically occurs during summer in the bottom waters of the PRE. Before the 2000s, it was an episodic and small-scale issue because of the synergetic effect of shallow topography, high turbidity (Ma et al., 2022), and the intermittent stratification due to periodic disturbance by the tides. However, large-scale occurrences of low oxygen (when DO < 4 mg/L) and hypoxia were frequently reported in recent years. For example, it was estimated that the low-oxygen area within the PRE achieved 1000 km² and 1500 km² during summer in 2010 (Wen et al., 2020) and 2015 (Li et al., 2018), respectively, which were nearly double to that before the 2000s (Li et

al., 2020). Hu et al. (2021) compiled historical observations over four decades to investigate the long-term deoxygenation trend and its spatial expansion in the PRE. They highlighted the significant contributions of increased nutrient and decreased sediment fluxes from the Pearl River to the exacerbation of low-oxygen conditions in the region. Besides, the low-oxygen inflows from the Pearl River could also contribute to the low-oxygen area in the upper estuary (Hu et al., 2021). Nevertheless, a quantitative understanding of their relative contributions to the low-oxygen expansion in the PRE is lacking, particularly in different subregions (Fig.1b) where the mechanisms controlling the low-oxygen conditions are different. In the upper part of the PRE (Lingdingyang waters), aerobic respiration of terrestrial organic matter plays a greater role (Su et al., 2017; Yu et al., 2020); in the downstream regions of the PRE, deoxygenation is primarily controlled by eutrophication (Yu and Gan, 2022; Chen et al., 2024).

In this study, we used a coupled physical-biogeochemical model to investigate the decadal changes (the 1990s versus the 2010s) in summertime DO contents and related

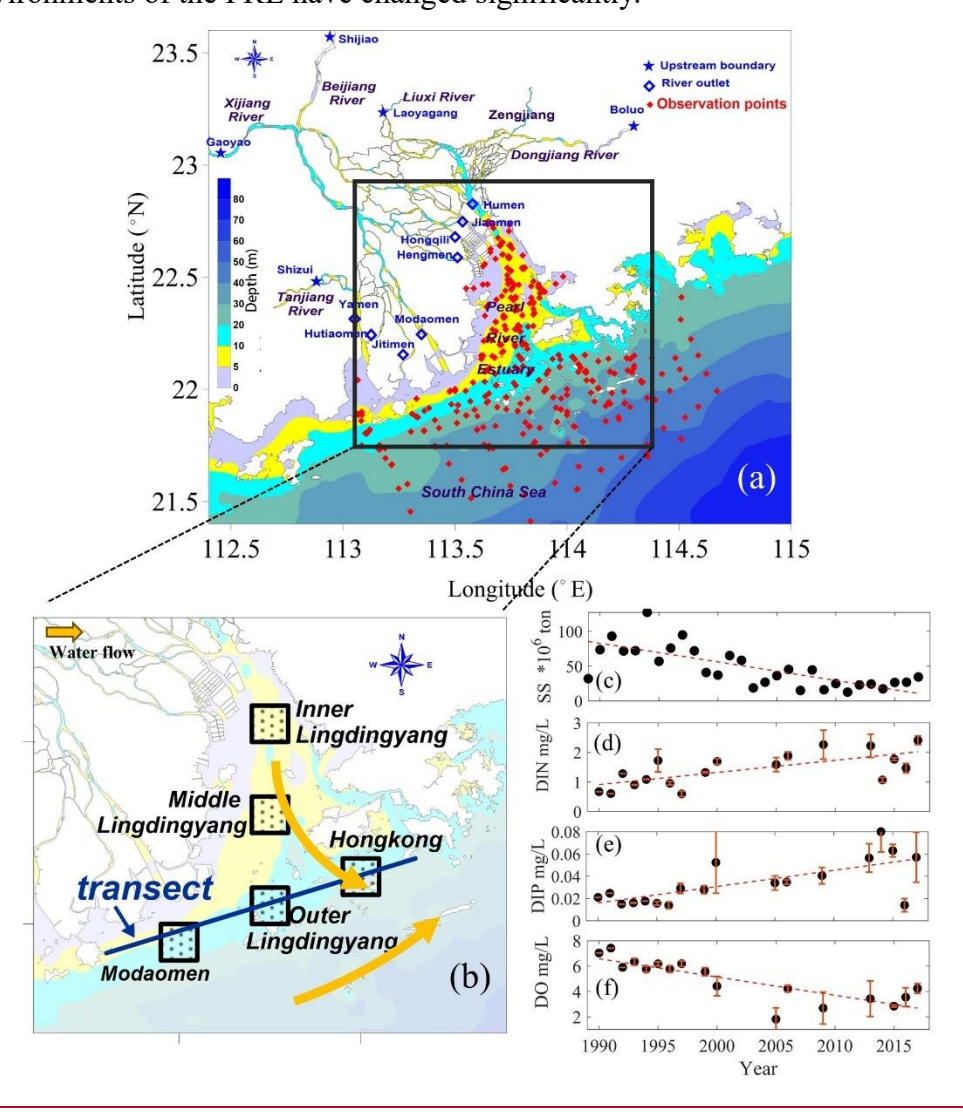
In this study, we used a coupled physical-biogeochemical model to investigate the decadal changes (the 1990s versus the 2010s) in summertime DO contents and related biogeochemical processes in the PRE and to quantify the relative contributions of the changing riverine inputs (including nutrients, suspended sediments, and oxygen content; Fig. 1c-f) to the long-term expansion of low oxygen (DO < 4 mg/L) and hypoxia (DO < 3 mg/L) in the region.

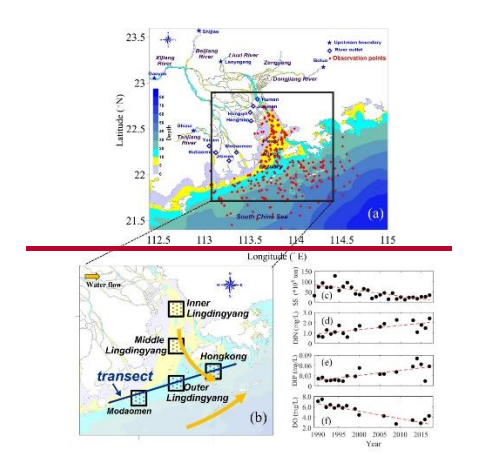
2. Material and methods

2.1 Study area

The PRE and its adjacent shelf waters (Fig. 1a) represent an estuarine system under intensive human activities. One major anthropogenic impact in the PRE is the terrestrial substances fed by the Pearl River, which is the third largest river in China with an average annual runoff of 3.26×10^{11} m³/ Year (Luo et al., 2002), through eight river outlets, including Humen, Jiaomen, Hongqili, Hengmen, Modaomen, Jitimen, Hutiaomen, and Yamen (Fig. 1a). The long-term DO and water quality data used here

were collected from open sources (e.g. government websites) and published studies (detailed in Data availability and Table S1 of Supplement). Over the past few decades, the terrestrial inputs from the Pearl River have experienced remarkable changes in oxygen content, sediment loads, and nutrients including dissolved inorganic nitrogen (DIN) and dissolved inorganic phosphorus (DIP) (Fig. 1c-f). Consequently, the ecological environments of the PRE have changed significantly.





| | | | | | |

Fig. 1. (a) Study area of the PRE and sampling sites during 1985-2017; (b) <u>fF</u>ive subregions and a transect along the coastal transition zone used for analysis and the <u>surface</u> water flow direction—in the <u>surface</u> water; (c) <u>aA</u>nnual loads of suspended sediments (SS) from the Pearl River—(The data source can be found in Table S1, Riverine SSC); (d-f) <u>Summer-averaged</u> (June to August) the surface-layer (within the upper 2 m of water column) <u>summertime</u>—concentrations of nutrients (DIN, DIP) and dissolved oxygen (DO)—at Humen Outlet (the primary monitoring site). Error bars indicate intrasummer variability across sampling dates in the river outlets of the PRE (The data source can be found in Table S1, Riverine DIN, DIP, DO).

DuringIn the 1990s, the Pearl River Estuary (PRE) experienced low eutrophication levels—displayed a low level of eutrophication levels, consistent with limited upstream urbanization and relatively high sediment loadsreflecting limited upstream urbanization at that time. This period sawalso witnessed extensive construction of water infrastructure—projects,—, mostly completed around—by 2000, including over 8,636 reservoirs in the Pearl River Basin (Wu et al., 2016), which drove a significant decline in riverine suspended sediment concentration (SSC)—(Zhang et al., 2008), which led to a dramatic reduction in the riverine suspended sediment concentration (SSC). By the late 1990s, the Pearl River basin contained at least 8636 reservoirs (Wu et al., 2016). After the 2000s, with the acceleratedion of urbanization and continued construction of hydraulic development further altered river inputs, with monitoring data showing decreased sediment loads (Fig. 1c) and increased nutrient concentrations (Fig. 1d—e). These changes collectively enhanced facilities, the PRE has

undergone a significant increase in nutrients and decline in sediment loads (Fig. 1c e), both of which are favorable for phytoplankton blooms potential, exacerbating and therefore for eutrophication and hypoxia. These long-term variations of riverine substances have also been reported by Lai et al. (2022) and Hu et al. (2021). In the meantime, the oxygen content in the PRE has exhibited a notable drawdown with significant expansions in low-oxygen extents in recent summers (Fig. 2), which has been revealed by the cruise observations in the PRE (Li et al., 2021; Su et al., 2017; Hu et al., 2021; Lu et al., 2018).

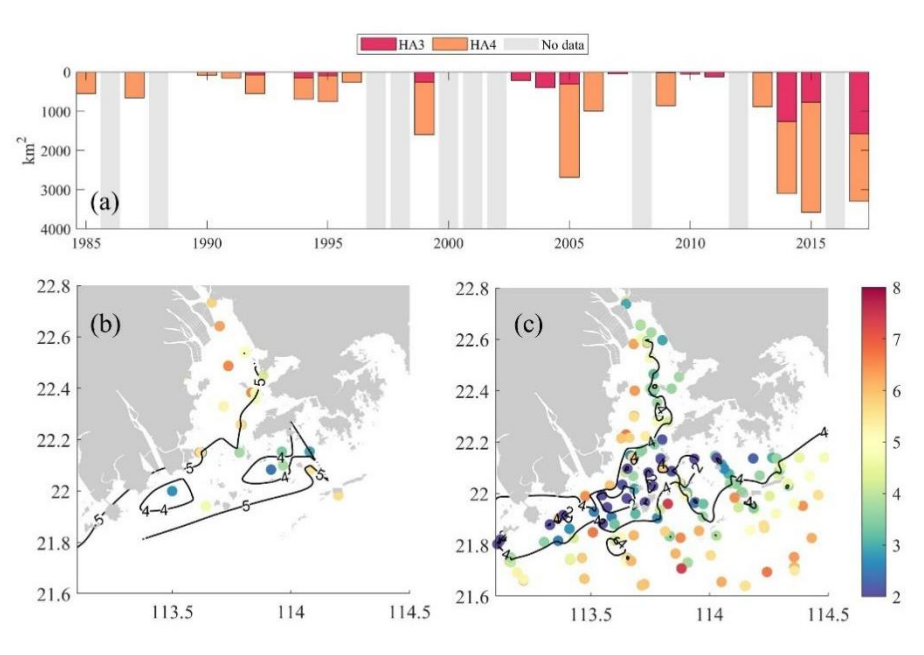


Fig. 2. (a) Interannual variations of low-oxygen area (HA4, DO < 4 mg/L) and hypoxic area (HA3, DO < 3 mg/L) in the bottom waters (~1-2 m above sediments) of the PRE, calculated via liner interpolation on a 0.01° × 0.01° grid using summer cruise observations during summer estimated from the cruise observations (note that the grey patches indicate data gapsrepresent the lack of data).; spatial Spatial distributions of summer-averaged bottom DO concentrations during (b) 1991-1996 and (c) 2013-2017.

2.2 Model settings and validation

2.2.1 Model descriptions and settings

An online 1D-3D coupled physical-biogeochemical model, which has been extensively verified and applied in the PRE (Wang et al., 2017; Wang et al., 2018; Hu et al., 2011; Zhang et al., 2022), was utilized here to reproduce the oxygen dynamics

under the long-term changes in riverine nutrients, suspended sediment concentration (SSC), and oxygen content (Fig. 1c-f). This 1D-3D modeling framework integrates a 1D representation of the Pearl River network with a 3D simulation of the Pearl River Estuary and adjacent shelf region, operating in an offline online coupling mode. The 1D component numerically solves the Saint-Venant equations using a Preissmann scheme, discretizing the river network into 299 sections with five upstream boundaries (specified as either discharge or water level inputs). The 3D component employs the ECOM model with 16 vertical layers and adaptive horizontal resolution (400m to 3km), forced by tides, atmospheric forcing, and open boundary conditions. The two components exchange fluxes at eight river outlets: the 3D model incorporates river discharge from the 1D model as upstream boundary conditions, while the 1D model uses water levels computed by the 3D model as its downstream boundaries at each time step. This 1D-3D modeling framework was initially developed to investigate nutrient fluxes to the PRE and has been extended and validated to simulate oxygen dynamics and hypoxia in the PRE (Wang et al., 2017; Wang et al., 2018; Hu et al., 2011; Zhang et al., 2022; Chen et al., 2024). For the sake of conciseness in the main text, detailed descriptions on the physical and suspended sediment modules were provided in the Supplement (Text S1). Regarding the biogeochemical module, it is based on the Row-Column Aesop (RCA), which simulates interactive cycles of oxygen, carbon, nitrogen, phosphorus, and silicon in the water column (HydroQual, 2004). As for the oxygen dynamics, it can be described as follows: The schemes for DO dynamics and phytoplankton growth in the model can be found in previous studies (Wang et al., 2017; Wang et al., 2018). $\frac{\partial DO}{\partial t} = -\mathbf{u} \cdot \nabla DO + \nabla \cdot (\mathbf{D} \nabla DO) + Rea + Phot + WCR + SOD$ where the velocity vector u = (u, v, w), ∇DO represents the gradient operator (spatial derivative of dissolved oxygen concentration), and D is the diffusion coefficient tensor.; Rea and Phot, WCR, and SOD represent the rates of air-water oxygen exchange, photosynthesis, water column respiration, and sediment oxygen demand, respectively

192

193

194

195

196

197

198

199

200

201

202

203

204

205

206

207

208

209

210

211

212

213

214

215

216

217

218

220 (unit: mg O₂ L⁻¹day⁻¹). The air-water oxygen exchange is parameterized as:

$$221 Rea = K_a \theta_a^{T-20} \cdot (D\theta_{sat} - D\theta) (2)$$

- where K_a is the surface mass transfer coefficient (m/day), θ_a is the temperature
- 223 coefficient, T is the water temperature, and DO_{sat} is dissolve oxygen saturation
- 224 concentration. The SOD is calculated by the sediment flux module (SFM) coupled to
- the RCA. The sediment module simulates the sedimentation and remineralization of
- 226 organic carbon, nitrogen, and phosphorus, and dynamically estimates the oxygen and
- 227 nutrient fluxes across the sediment-water interface (Fizpartick, 2004).
- The growth of phytoplankton is co-limited by temperature, light, and nutrient
- 229 conditions. The calculation of gross primary production (GPP, mg C L⁻¹ day⁻¹) of
- 230 phytoplankton is determined as:

231
$$GPP = G_{pmax} * e^{-\beta(T_{opt} - T)^2} * G_N(N) * G_I(I) * P_c$$
 (3)

- 232 where G_{rmax} is the maximum grow rate of phytoplankton at the optimum temperature
- 233 (day⁻¹); T_{opt} is the optimum temperature (°C); β is the shaping coefficients; T is the
- water temperature (°C); $G_I(I)$ is the light limitation factor; $G_N(N)$ is the nutrient
- limitation factor; P_{ϵ} is the phytoplankton biomass (mg C L⁻¹).
- The nutrient limitation factor $(G_N(N))$ is parameterized as:

$$237 G_N(N) = Min\left(\frac{DIN}{K_{mN} + DIN}, \frac{DIP}{K_{mP} + DIP}, \frac{Si}{K_{mSi} + Si}\right) (\underline{14})$$

- where DIN, DIP, and Si represent the concentration (mg L⁻¹) of dissolved inorganic
- 239 nitrogen (including NO₃- and NH₄+), dissolve inorganic phosphorus (PO₄3-), and
- dissolve inorganic silicon (SiO₃²⁻), respectively; K_{mM} , K_{mR} , and K_{mSI} represent the
- half-saturation constants (mg L⁻¹) for DIN, DIP, and Si, respectively. It should be noted
- 242 that a higher nutrient limitation factor $G_N(N)$ indicates a weaker nutrient limitation
- 243 effect on phytoplankton growth. Moreover, the nitrogen and phosphorus limitation are
- 244 more significant than silicon limitation within the PRE, thus this study mainly focuses
- 245 on the former.
- where DIN, DIP, and Si are concentrations (mg L⁻¹) of dissolved inorganic nitrogen
- 247 (NO₃⁻, NH₄⁺), phosphorus (PO₄³⁻), and silicon (SiO₃²⁻), respectively. K_{mN} , K_{mP} , and

- K_{mSi} are their corresponding half-saturation constants. A higher $G_N(N)$ indicates
- weaker nutrient limitation. Given the stronger N and P limitation compared to Si in the
- Pearl River Estuary (PRE), this study emphasizes N and P.
- The light limitation factor $G_I(I)$ is parameterized as:

252
$$G_I(I) = \frac{e}{k_e H} \left[\exp\left(\frac{-I_0(t)}{I_S} e^{-k_e H}\right) - \exp\left(\frac{-I_0(t)}{I_S}\right) \right]$$
 (25)

with the light extinction coefficient:

$$254 k_e = k_{ebase} + k_c * a_{cchl} * P_c + k_{sed} * SSC + k_{POC} * POC (36)$$

- and the surface light at depth:
- $256 I_0 = I_{surf} * e^{-k_e * H}$
- $257 \qquad ----(47)$
- Here, H is water depth (m), I_s the saturation light intensity (ly day⁻¹), I_{surf} is the
- surface light (ly day⁻¹), and the k-terms are light attenuation coefficients due to water,
- 260 Chl a, SSC, and POC.
- where H is the depth of water column (m); I_{tt} is the incident light intensity at the
- segment surface (ly day⁻¹); $I_{\mathfrak{s}}$ is the saturating light intensity (ly day⁻¹); $k_{\mathfrak{e}}$ is the light
- extinction coefficient (m⁻¹); k_{ebase} is the background light extinction coefficient of
- water (m⁻¹); k_{ϵ} is the phytoplankton-related extinction coefficient (m²-mg⁻¹ Chla); a_{cent}
- 265 is the ratio of chlorophyll to phytoplankton carbon biomass; k_{sed} is the SSC-related
- 266 extinction coefficient (m² mg⁻¹ SSC); k_{POC} is the POC-related light extinction
- 267 coefficient (m²-mg²-POC); I_{surf} is the instantaneous light radiation received at the
- 268 water surface (ly day⁻¹).
- To estimate the spatial characteristics of light conditions, we also calculated the
- eutrophic depth in the PRE ($H_{\underline{E}}$, Equation 8), which is defined as the water depth
- reached by 1% of the surface light intensity (I_{surf}) . Basically, a larger eutrophic depth
- indicates a better light condition for phytoplankton growth. To assess light conditions,
- 273 the eutrophic depth H_E is computed as the depth where light is 1% of surface intensity:

$$I_{surf} * e^{-k_e * H_E} = I_{surf} * 1\%$$
 (85)

276

2.2.2 Model validation

The coupled physical-biogeochemical model mentioned above has already been
validated against a variety of observations for several periods, which showed good
performance in reproducing the physical conditions, suspended sediment dynamics,
and biogeochemical cycles in the PRE. We briefly summarized the validation results
here. For the physical and suspended sediment modules, Hu and Li (2009) has applied
the 1D-3D coupled model to establish 30-day realistic simulations for July 1999 and
February 2001. The simulated water levels, discharges, salinity, and SSC agreed well
with the observations in the Pearl River network and the PRE for both periods, with
correlation coefficients all greater than 0.65 in summer. The simulated SSC at the
surface was also compared to satellite remote sensing data, which showed a fairly close
spatial pattern and comparable concentration magnitude. Furthermore, Wang et al.
(2017) provided an extensive model validation using field data collected from four
seasonal cruises in 2006, with high correlations for water levels (> 0.95), salinity (>
0.90) and temperature (> 0.80) and low root-mean-standard-errors between the
simulation and observations in summer.
Then, the biogeochemical module was established and used to explore the nutrient
and oxygen dynamics off the PRE in July 1999 and January-December 2006 (Hu and
Li, 2009; Wang et al., 2017). Detailed model settings and parameters can be found in
Wang et al. (2017). For validation, The point-to-point comparisons with the water
quality data from cruise surveysprofiles indicated that the biogeochemical module was
robust to reproduce the spatial distributions of <u>nutrientammonia</u> , <u>nitrate</u> , <u>phosphorus</u> ,
<u>chlorophyll a, and oxygen concentrations, and ehlorophyll a in the PRE (Figs. 3, 5)</u> . <u>To</u>
further assess light attenuation dynamics, we obtained diffuse attenuation coefficient at
100 nm (K (100)) data for the PRE from the ELIMETSAT Ocean color Thematic

Assembly Centre (https://www.oceancolour.org/). We converted $K_d(490)$ to photosynthetically active radiation attenuation coefficient (K_{par}) using the empirical formula proposed by Lee et al. (2005), and then calculated the euphotic depth using Eq. 5 in Section 2.2.1. Model-simulated and satellite-derived euphotic depths show close agreement in both the 1990s and 2010s (Fig. 4b, d), demonstrating consistent model performance across decades.

For hypoxia simulation, the Our model demonstrated strong validation performance by accurately capturing captured the observed temporal expansion of hypoxia, transitioning from localized bottom hypoxia in the 1990s (Fig. 2b-c) to widespread occurrences in the 2010s (Fig. 5d-e). Initial validation against 1994-1999 summer observations showed close agreement, with simulated low-oxygen (HA4=1179.7 km²) and hypoxic (HA3=211.3 km²) areas matching observational estimates (802±437 km² and 131±84 km²; Fig. 2a, Table 3). For the 2013-2017 period, the model successfully replicated hypoxia intensification, as evidenced by HA4 expansion to 2925.5 km² aligning with observed 2715±1068 km². Projections to Reproduction of For the 20120s, simulated indicated HA3 doubleding to 617.2 km², consistent remaining with in observational uncertainty ranges (901±591 km²; 2013-2017 data). These results collectively, confirming the model's robustness in simulating both historical patterns and emerging hypoxia dynamics. In addition, Wang et al. (2017) has compared the simulated oxygen kinetic terms (including the air-sea re-aeration rate, water-column respiration and production rates, and sediment oxygen demand) with observations in summer, which demonstrated the model's capability in representing the important oxygen source-sink processes (e.g., oxygen consumptions across the sediment-water interface) in the PRE. Detailed model settings and parameters can be found in Wang et al. (2017).

2.3 Model experiments

304

305

306

307

308

309

310

311

312

313

314

315

316

317

318

319

320

321

322

323

324

325

326

327

328

329

330

Based on the well-validated model run in 2006 (Wang et al., 2017), the present study

performed diagnostic simulations for two representative periods, characterized by low nutrients and high suspended sediments and oxygen content during 1991-1996 (referring as to the "1990s case"; Table 1) versus high nutrients and low suspended sediments and oxygen content during 2013-2017 (referring as to the "2010s case"). Each case was run from 1 January to 31 August, driven by climatological physical conditions (freshwater discharges and wind speeds detailed in Text S1 of the Supplement) averaged over 1990-2017 and by mean observed values of riverine water quality components in the corresponding period. Specifically in summertime (a period used for formal analysis here), the riverine concentrations were set to 1.0 mg/L (DIN), 0.02 mg/L (DIP), and 6.5 mg/L (DO) in the 1990s case, while they were set to 2.0 mg/L, 0.065 mg/L, and 3.5 mg/L in the 2010s case (Table 1). The riverine SSC was specified at 40 mg/L in the 2010s according to the in-situ observation near the Humen outlet in 2015 summer (Chen et al., 2020), and was set to 100 mg/L in the 1990s based on the ratio of the sediment loads between the 1990s and the 2010s (2.5 times). The riverine boundary conditions for DIN, DIP, DO, and SSC during summertime are listed in Table 1 for both the 1990s and 2010s cases. Notably, the 2010s SSC was set based on field data (Chen et al., 2020), whereas the 1990s SSC was back-calculated from the 2.5-fold difference in sediment loads. Long-term monitoring at river outlets showed no significant temporal trend in chemical oxygen demand (COD) compared to the marked increases in nutrients and decreases in DO (Lai et al., 2022), indicating stable oxygenconsuming organic matters (OM) inputs. We therefore maintained constant OM concentrations between study periods (organic carbon: 2 mg/L; organic nitrogen: 0.2 mg/L; organic phosphorus: 0.03 mg/L), consistent with published historical observations (Wang et al., 2018). Furthermore, three additional model scenario simulations were conducted in order to disentangle the individual impact of each varying riverine input on the summer deoxygenation off the PRE. The setting of each scenario was identical to that of the 1990s case except that the riverine nutrients, SSC, and DO were separately replaced by the representative value in the 2010s (referring as

331

332

333

334

335

336

337

338

339

340

341

342

343

344

345

346

347

348

349

350

351

352

353

354

355

356

357

to the "High-nutrient case", "Low-SSC case", and "DO-restore case", respectively;

Table 1)

Table 1. Riverine inputs (in unit of mg L-1) for model experiments.

Cases	DIN	DIP	DO	SSC
1990s	1.0	0.020	6.5	100
2010s	2.0	0.065	3.5	40
High-nutrient	2.0	0.065	6.5	100
Low-SSC	1.0	0.020	6.5	40
DO-restore	2.0	0.065	6.5	40

3. Results

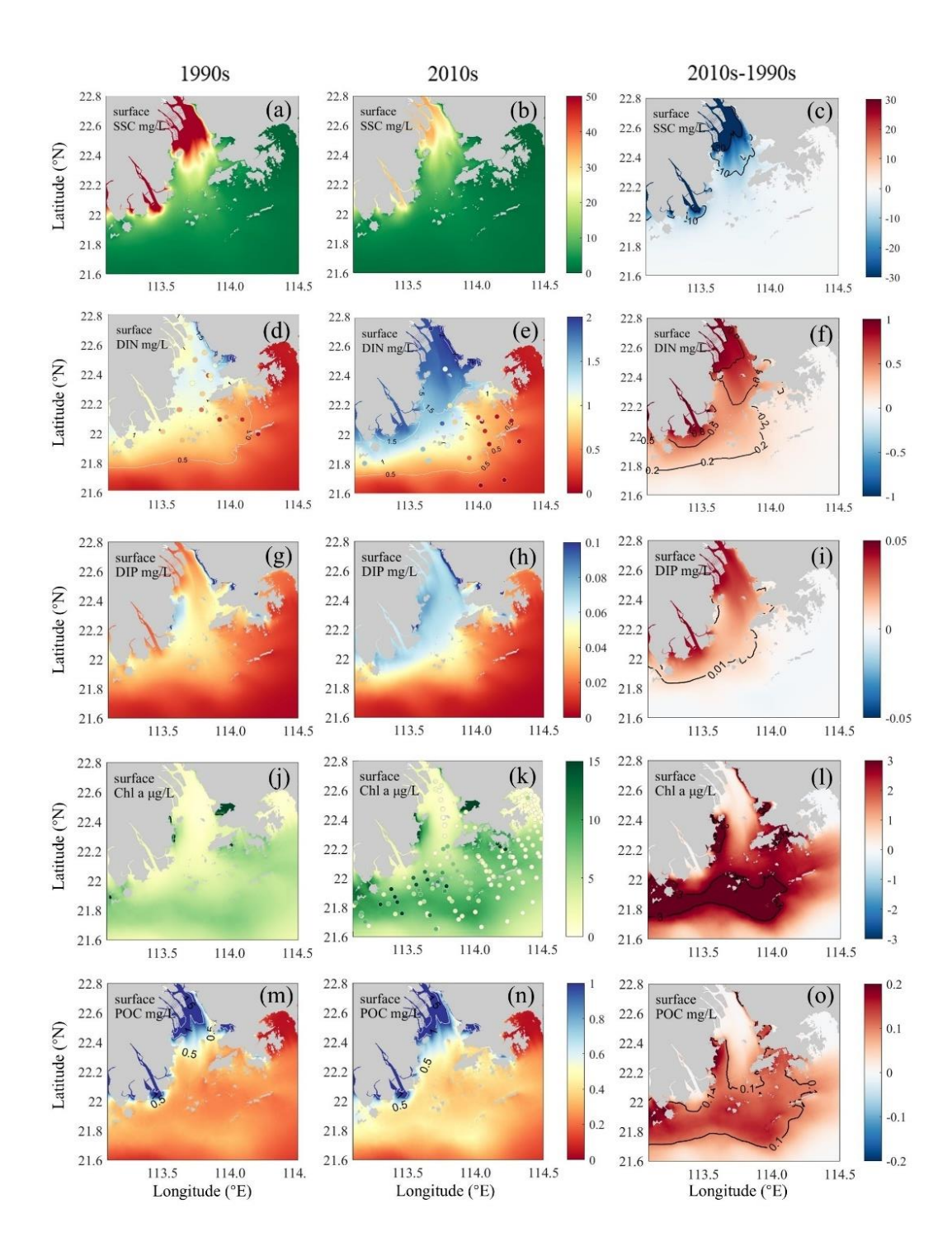
3.1 Responses of eutrophication to human-induced changes in the PRE

3.1.1 Long-term variations in water quality distributions

To examine changes in eutrophication (a key process affecting DO dynamics) and its influential factors during summer in the PRE, we compared the simulated distributions of SSC, nutrients, Chl *a*, and POC in the surface waters between the 1990s and the 2010s cases (Fig. 3) as well as their vertical integrations in subregions (Table 2). Model results showed that the surface SSC within the PRE largely declined during the two periods. In the 1990s, SSC maintained at a high level in the inner Lingdingyang Bay (see its location in Fig. 1b), ranging from 70.0 to 100.0 mg/L (Fig. 3a). Due to the particle sinking as waters advected downstream, SSC decreased to ~10.0 mg/L in the lower reaches of the PRE in the 1990s. While in the 2010s, the riverine sediment loads have remarkably decreased, resulting in a corresponding drawdown in SSC downstream (Fig. 3b-c). Overall, the vertically-integrated SSC content in the inner Lingdingyang Bay and lower PRE dropped by 56.1% and 45.6%-47.3% to 244.5 mg/m² and 38.4-69.2 mg/m², respectively (Table 2).

In terms of nutrients, the variation induced by riverine inputs was also evident

during the two periods, acting on the main estuary in association with the spreading of the river plume. As shown, the DIN content in the 1990s was mostly below 1.5 mg/L within the entire PRE (Fig. 3d). With respect to the 2010s, the DIN concentration has increased by 0.8 mg/L and 0.2 mg/L in the surface waters of the upper Lingdingyang Bay and the lower PRE, respectively (Fig. 3e-f). The vertically-integrated DIN mass has increased by 41.9%-102% in the PRE (Table 2). A similar situation occurred with respect to DIP, with its content increasing from 0.04 mg/L in the 1990s to 0.07 mg/L in the 2010s in the high-DIP area adjacent to the middle Lingdingyang Bay (Fig. 3g-i). In terms of vertical integration, DIP increased by 9%-108%, with the lowest increases located in the Hong Kong waters downstream of the estuary (Table 2).



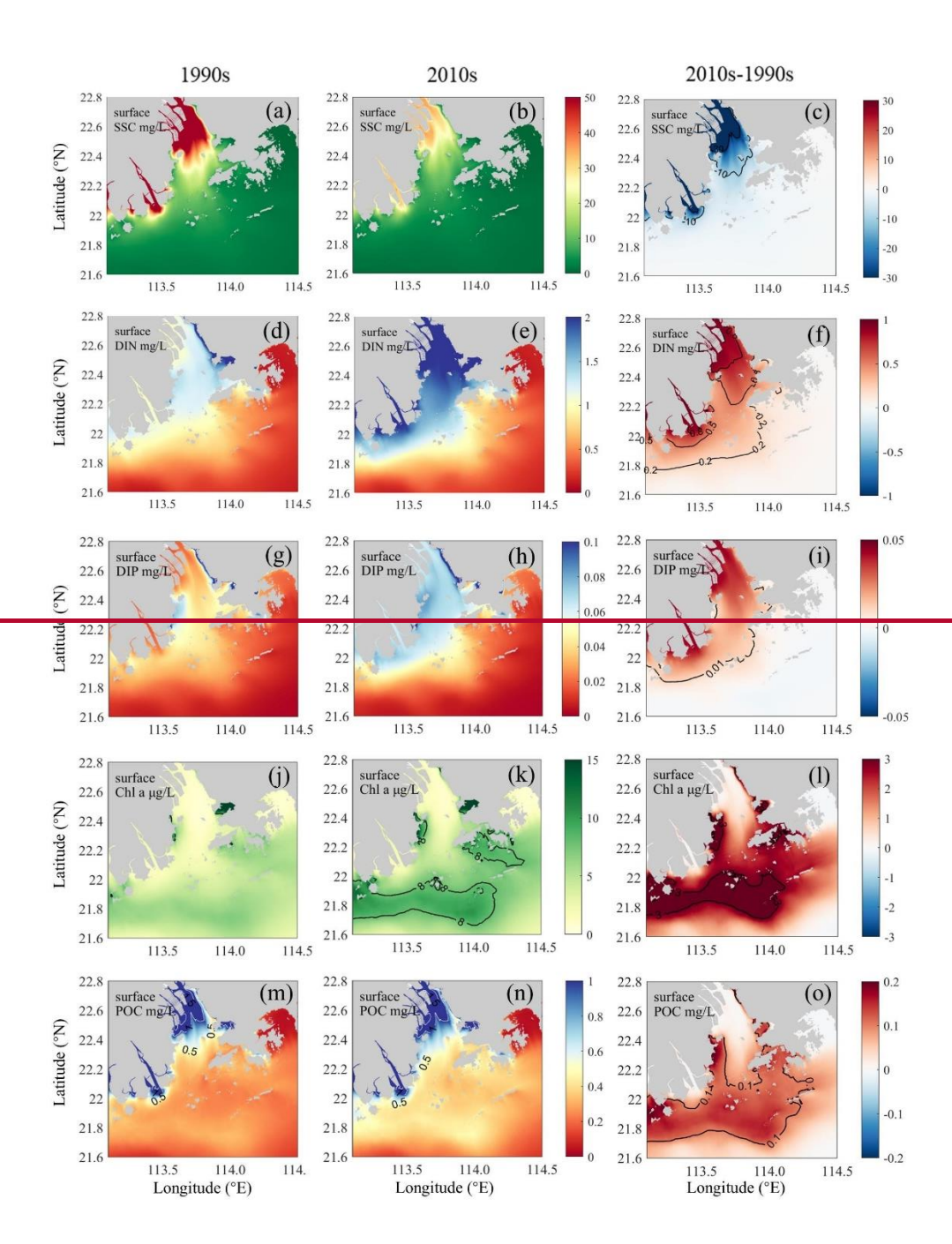


Fig. 3. Simulated <u>surface water</u> distributions <u>in the PRE for of (a-c) SSC</u>, (d-f) DIN, (g-i) DIP, (j-l) Chl a, and (m-o) POC concentrations. <u>Left panels (a, d, g, j, m) show 1990s</u> conditions, middle panels (b, e, h, k, n) show 2010s conditions, and right panels (c, f, i, l, o) show their differences (2010s-1990s). Corresponding observations are indicated by colored dots in DIN (d, e) and Chl a (j, k) panels. in the surface waters of the PRE for the 1990s (left panels) and the 2010s (middle panels) as well as their differences (right panels).

Table 2. Vertical integrations of DIN, DIP, SSC, Chl a, and POC contents; nutrient limitation index and euphotic depth; and DO concentrations, low-oxygen frequency (HF4), hypoxia frequency (HF3), and oxygen consumption rates in the bottom waters for subregions of the PRE (see locations in Fig. 1b) during the 1990s and the 2010s.

Culturaciona	Inner		Middle		Modaomen	en	Outer		$o_A v_{ao}\Pi$	on axiotomo
Subregions	Lingdingyang Bay	ang Bay	Lingding	Lingdingyang Bay	sub-estuary	ıry	Lingding	Lingdingyang Bay	nollg No	nong wong waters
Cases	1990s	2010s	1990s	2010s	1990s	2010s	1990s	2010s	1990s	2010s
$DIN (mg m^{-2})$	6.58	12.24	5.42	9.20	4.89	7.62	5.17	7.92	3.62	5.14
$DIP (mg m^{-2})$	0.23	0.48	0.34	0.48	0.55	0.71	0.56	99.0	0.51	0.56
Nutrient limitation index 0.94	0.94	0.97	0.95	0.97	0.92	0.94	0.91	0.93	0.83	0.85
$SSC (mg m^{-2})$	556.5	244.5	332.9	164.6	120.4	63.4	127.7	69.2	9.07	38.4
Euphotic depth (m)	-1.3	-2.3	-2.0	-4.2	-9.5	-11.2	-11.8	-15.2	-20.7	-21.0
$\mathrm{Chl}\ a\ (\mu\mathrm{g}\ \mathrm{m}^{-2})$	5.0	7.1	11.7	22.9	39.4	70.4	40.7	72.9	74.3	108.9
$POC (mg m^{-2})$	9.8	8.64	4.8	5.31	4.82	6:39	5.33	6.85	6.21	7.91
Bottom DO (mg L ⁻¹)	4.55	3.52	4.31	3.90	3.50	2.84	4.96	4.12	4.36	3.52
HF4	25.0%	79.7%	26.8%	65.2%	84.5%	99.1%	4.5%	49.3%	20.5%	61.1%
HF3	6.5%	27.6%	4.8%	10.1%	25.2%	%5.95	3.5%	9.1%	4.8%	21.4%
$WCR~(mg~O_2L^{\text{-}1}~day^{\text{-}1})$	-0.38	-0.45	-0.20	-0.25	-0.09	-0.11	-0.07	-0.09	-0.06	-0.07
$SOD (mg O_2 L^{\text{-}1} day^{\text{-}1})$	-1.72	-1.62	-0.89	-0.89	-0.24	-0.46	-0.28	-1.12	-0.91	-1.48

Note: HF4 (frequency of DO < 4 mg L⁻¹); HF3 (frequency of DO < 3 mg L⁻¹).

The euphotic depth is measured as negative values increasing downward downward-from the sea surface, with depth values defined as negative.

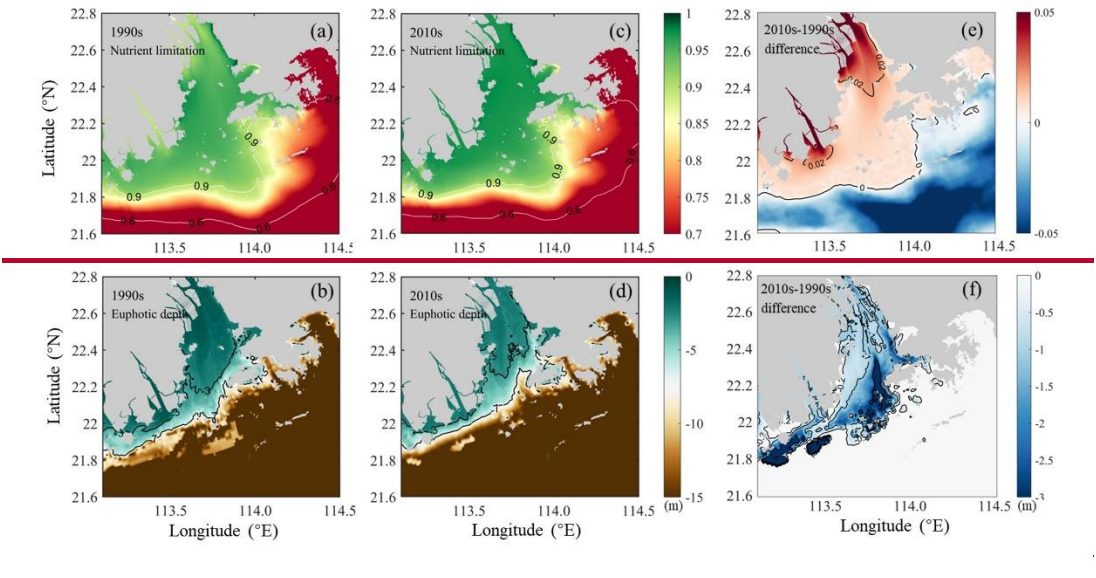
In response to changes in light (affected by the SSC content) and nutrient conditions, phytoplankton biomass has substantially grown in the 2010s, indicated by the increased Chl a concentration. In the 1990s, the phytoplankton biomass was at a low level, with the Chl a generally below 8.0 µg/L in the surface waters (Fig. 3j). As for the 2010s, significant phytoplankton blooms were found along the Modaomen subestuary, outer Lingdingyang Bay, and Hong Kong waters (Fig. 3k-l), with the vertically-integrated Chl a content rising by 31.0 µg/m² (by 78.7% compared to the 1990s), 32.2 µg/m² (79.1%), and 34.6 µg/m² (46.6%), respectively (Table 2). As a result of the elevated primary production, a great amount of organic matter was produced in the PRE. Spatially coupled to the growth of Chl a (Fig. 3l), the POC content has significantly increased in the 2010s, especially in the lower PRE (Fig. 3m-o), with the vertically-integrated concentration increasing by 1.5-2.0 mg/m² (by 27.4%-32.6% compared to the 1990s) over the water column (Table 2).

3.1.2 Long-term variations in nutrient and light limitations

The primary production in the PRE was controlled by the synergistic effects of nutrient and light conditions. We calculate the nutrient limitation factor and the eutrophic depth to quantify the intensity of nutrient limitation and light limitation on algae growth. It should be noted that a smaller nutrient limitation index and a shallower eutrophic depth represent a stronger nutrient limitation and a stronger light limitation, respectively. Results showed that the nutrient limitation exhibited a distinct estuary-shelf gradient, in which the Hong Kong waters experienced more severe nutrient limitation than the Modaomen sub-estuary and Lingdingyang Bay (Fig. 4a, c). Specifically, the nutrient limitation index decreased from the upper estuary (0.94) to the Hong Kong waters (0.83) in the 1990s. ByIn contrast, the light limitation has attenuated along the river plume transport pathway (Fig. 4b), largely ascribed to the decreaseding SSC (Fig. 3a-b). Both observations and model simulations revealed consistent spatial patterns. Compared to the Hong Kong waters, the regions adjacent to river outlets with underwent more severe light limitation, shown by the eutrophic depth progressively (Fig.

4b) increasing from <u>severely light-limited regions near river outletsthe</u> (Lingdingyang Bay-: (1.3 m;) and Modaomen sub-estuary-: (9.5 m) to the <u>less-limited</u> Hong Kong waters (20.7 m; Fig. 4b).







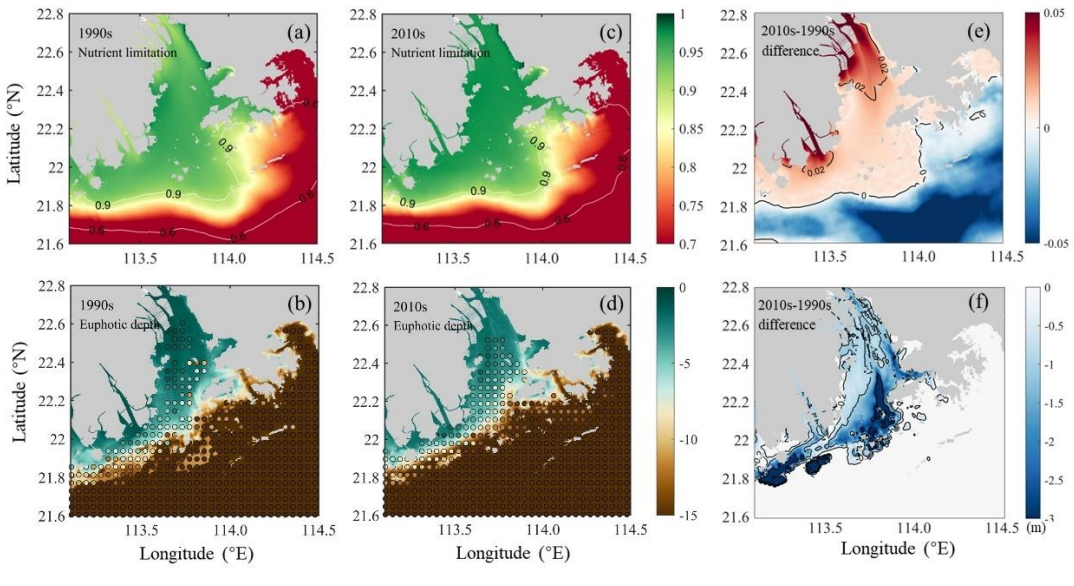


Fig. 4. Comparisons of (a, c) sSimulated distributions (a, e) and difference (e) of nutrient limitation index for the growth of phytoplankton growth and in the 1990s and the 2010s; (b, d) euphotic depths (in meters) between the 1990s and the 2010s, with their and its differences shown in (e) and (f), respectively. Colored dots in (b) and (d) represent corresponding euphotic depth observations. Note: Euphotic depth is measured as negative values increasing downward from the sea surface; thus, more negative differences in (f) indicate deeper light penetration in the 2010s. (in unit of m) in the 1990s and the 2010s. (The euphotic depth is measured downward from the sea surface,

with depth values defined as negative.)

The increased Due to the growth in nutrient loads, in the 2010s alleviated nutrient limitation was relieved in the 2010s. For instance, the nutrient limitation index in-the Hong Kong waters has increased to 0.85 (by a 2.4% increase from of the 1990s levels;) in the 2010s (Table 2). By contrastIn comparison, the relief of light limitation due to the reduced riverine suspended sediments was more evident. Both model simulations and observations revealed significantly greater with the reduced riverine suspended sediments. The deepening of the euphotic depth in the Lingdingyang Bay compared towas significantly greater than that in the lower estuary (Fig. 4b, d, f). In the inner Lingdingyang and middle Lingdingyang Bays, the euphotic depth increased by 1 m and 2.2 m (by 76.9% and 110.0% relative to the 1990s, Table 2), respectively. The alterations in light conditions in the remaining area were relatively minor, with the eutrophic depth increasing to 11.2 m (by 17.9%) in the Modaomen sub-estuary and to 21 m (by 1.4%) in the Hong Kong waters during the 2010s (Table 2).

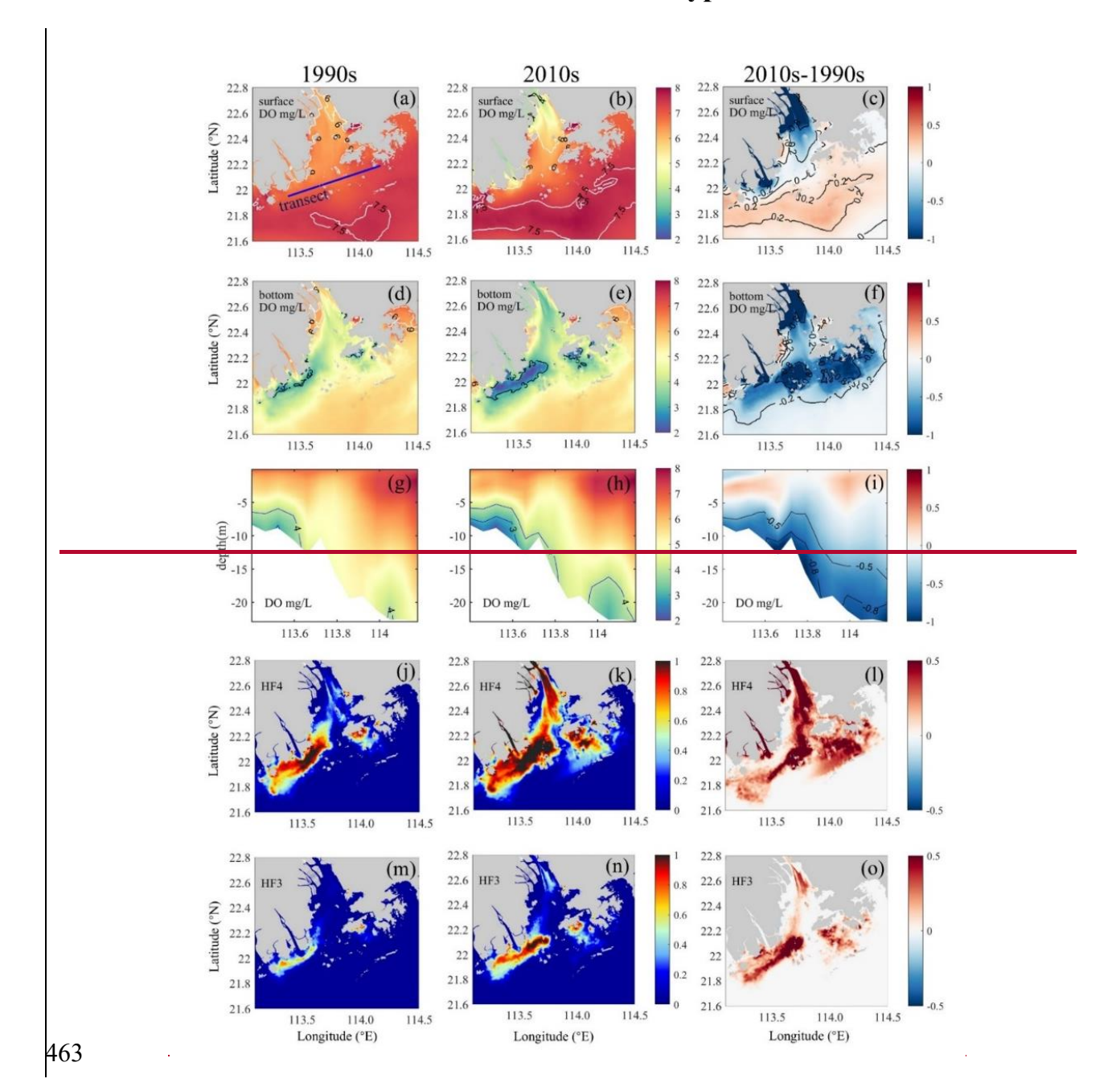
3.2 Responses of DO dynamics to human-induced changes in

461 the PRE

460

462

3.2.1 Variations in DO distributions and hypoxia occurrences



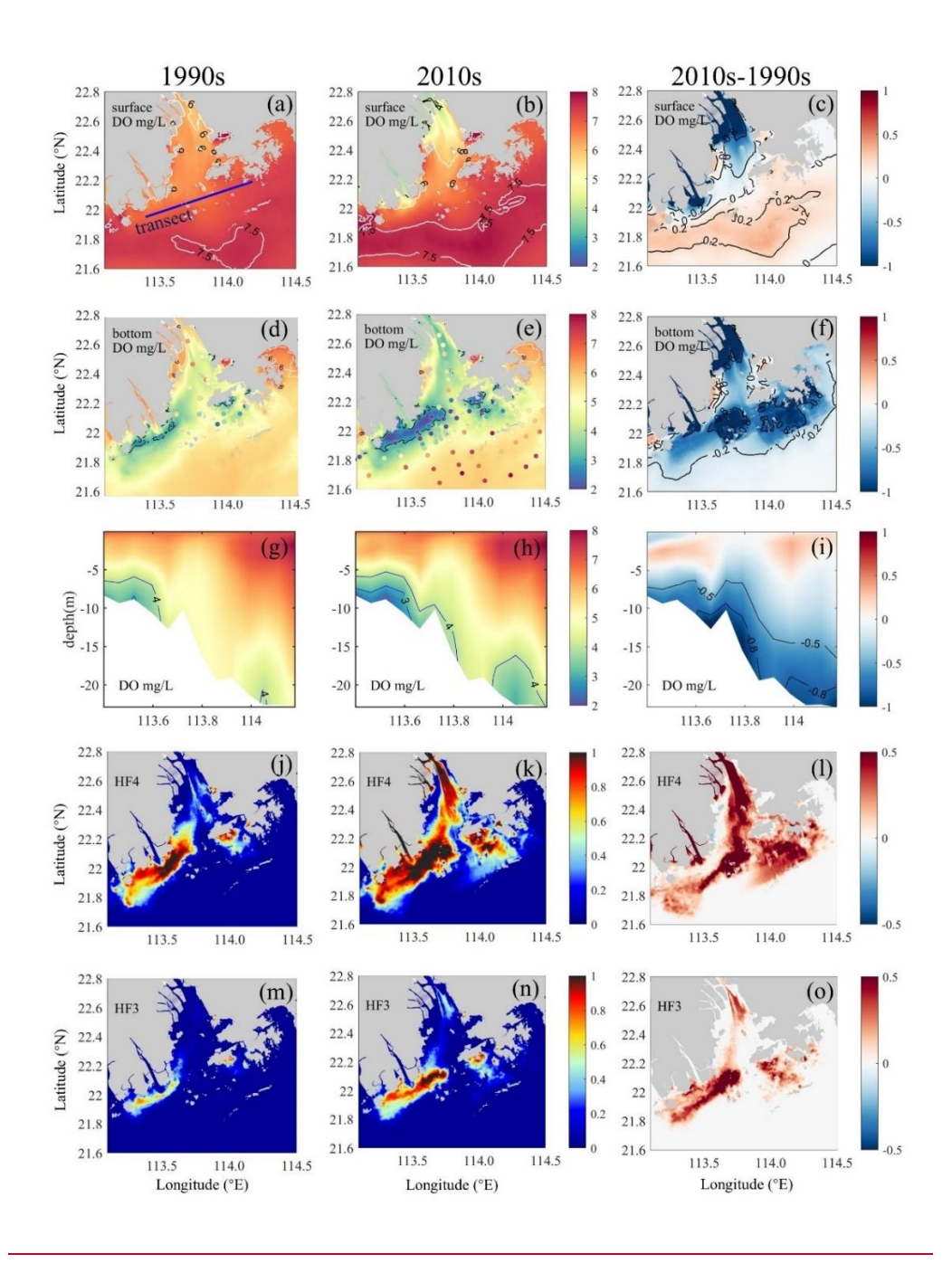


Fig. 5. (a-c) Surface DO and (d-f) bottom DO distributions, (g-i) vertical DO distributions along the transect (see its location in panel a), and (j-l) low-oxygen frequency (HF4, DO < 4 mg/L) and (m-o) hypoxia frequency (HF3, DO < 3 mg/L) in the bottom waters of the PRE for the 1990s (left panels) and the 2010s (middle panels) as well as their differences (right panels). Note that hypoxia frequency is calculated as the number of hypoxic days divided by the total number of days in the study period, yielding a dimensionless ratio (range: 0–1).

473 474

475

476 477 478

479 480

482 483 484

481

485

486 487

488 489

490

491

492

493

494

495

496

497

Our model revealed distinct temporal shifts in summertime DO patterns and hypoxia distribution (Fig. 5). The 1990s surface waters generally maintained DO >6 mg/L, increasing toward shelf regions (Fig. 5a). By the 2010s, surface DO increased increase by 0.2-0.3 mg/L (Fig. 5b-c), with an oxygen-enriched zone in the lower PRE correlating with high Chl a (Fig. 3k), though new low-oxygen zones (DO <4 mg/L) emerged near river outlets due to reduced Pearl River DO influx.

Bottom water simulations captured the hypoxia expansion from localized 1990s events (Fig. 2b-c) to widespread 2010s occurrences (Fig. 5d-e). Initial hypoxia clustered along the western PRE (Modaomen sub-estuary; Fig. 5d), with simulated HA4 (1179.7 km²) and HA3 (211.3 km²) (Table 3) matching observations (802±437 km² and 131±84 km²; 1994-1999 summers; Fig. 2a). By the 2010s, hypoxia intensified throughout Lingdingyang Bay and Hong Kong waters, with bottom DO declining to 2.8-4.1 mg/L (Table 2). Simulated HA4 expanded 1.5-fold to 2925.5 km² (Table 3), consistent with observed 2715±1068 km² (2013-2017; Fig. 2a). HA3 doubled to 617.2 km^2 by the $\frac{2020s}{2010s}$, comparable to observed $901\pm591 \text{ km}^2$ (2013-2017).

Table 3. Simulated low-oxygen (HA4, DO < 4 mg/L) and hypoxic (HA3, DO < 3 mg/L) areas in the bottom waters of the PRE and their changes relative to the 1990s

17703.				
Cases	HA4 (km²)	Percentage of	HA3 (km ²)	Percentage of
Cases	11A4 (KIII)	change	IIA3 (KIII)	change
1990s	1179.7	/	211.3	/
2010s	2925.5	+148%	617.2	+192%
High-nutrient	1542.6	+31%	282.5	+34%
Low-SSC	1737.0	+47%	412.4	+95%
DO-restore	2409.7	+104%	617.2	+192%

Note: The calculation in percentage of change is: (HA_x-HA_{1990s}) / HA_{1990s} , where x represents each case.

centers along the coastal transition zone (Modaomen sub-estuary and Hong Kong waters; Fig. 2b-c), revealing distinct spatiotemporal deoxygenation patterns (Fig. 5g-o). During the 1990s, both centers exhibited limited low-oxygen zones, with Hong Kong waters showing <1 m thick DO <4 mg/L layers (Fig. 5g). Low-oxygen (HF4) and hypoxic (HF3) conditions persisted 18-76 days (20.5%-84.5% frequency) and 4-23 days (4.8%-25.2%) respectively during summer months (Fig. 5j,m; Table 2).

By the 2010s, hypoxic thickness increased substantially to \sim 1.5 m at Modaomen and \sim 5 m (\sim 4 m thicker than 1990s) at Hong Kong waters (Fig. 5h). Event durations prolonged to 55-89 days (61.0%-99.1% HF4) and 19-51 days (21.4%-56.5% HF3) respectively (Fig. 5k, n; Table 2), demonstrating intensified and prolonged hypoxia.

3.2.2 Variations in bottom oxygen consumption

To further explore the mechanism of long-term deoxygenation off the PRE, we investigated the oxygen consumption rates and their changes during the two periods (the 1990s versus the 2020s2010s). We specifically focused on the oxygen consumption at the bottom layers covering the 20% of the water depth above the sediments, where the majority of hypoxic events in the PRE occurred (Fig. 5).

As shown in Table 2, the predominant oxygen sink in the bottom waters of the PRE was sediment oxygen demand (SOD) induced largely by the remineralization of organic matter in sediments, whereas water column respiration (WCR) only accounted for 15.2% of the bottom oxygen consumption on average. Over the past three decades, both the WCR and SOD have generally increased in the PRE, primarily attributed to the growth in local production of organic matter associated with aggravated eutrophication (Fig. 3j-o). Particularly, the SOD in the outer Lingdingyang Bay and Hong Kong waters has remarkably increased from 0.28-0.92 mg O₂ L⁻¹ day⁻¹ in the 1990s to 1.12-1.48 mg O₂ L⁻¹ day⁻¹ in the 2010s (Table 2), which contributed to 80%~95% of the increment in total oxygen consumption. Although the absolute increase of SOD in the Modaomen sub-estuary was comparatively small, the SOD in the 2010s has

almost doubled compared to the 1990s, leading to a substantial increase in the occurrence of hypoxic events in this region (Fig. 5d-o).

526

527

528

529

530

531

532

533

534

535

536

537

538

539

540

541

542

543

544

545

546

547

548

549

550

551

552

3.2.3 Disentangling contributions of riverine oxygen, suspended sediments, and nutrient changes on deoxygenation

As detailed in Section 2.3, three scenario simulations were performed to quantify the relative contributions of riverine changes to the decadal low-oxygen expansion in the PRE (Table 1). In general, the riverine impacts on DO and related biogeochemical factors varied significantly between subregions (Figs. 6-7). Specifically, increasing the riverine nutrient levels from the 1990s to the 2020s 2010s alone (High-nutrient case) led to a marked drawdown in the bottom DO around the lower PRE (by over 0.2 mg/L relative to the 1990s; Fig. 6a). The DO decline, extending from the Modaomen subestuary to the Hong Kong waters, was ascribed to the elevated phytoplankton biomass (Fig. 7b) facilitated by better nutrient conditions, which subsequently sustained stronger bottom oxygen depletions compared to the 1990s (Fig. 7c). Among the subregions, the Hong Kong waters was more susceptible to the changes in riverine nutrients as it was subject to comparatively severe nutrient limitation (Table 2). Therefore, with the improvement of nutrient utilization, this region experienced more pronounced deoxygenation in association with significant alterations in Chl a content and SOD (increased by 14.2 μg/m² and 0.26 mg O₂ L⁻¹ day⁻¹, respectively, equivalent to 47.1% and 46.4% of their total increments over the past three decades; Fig. 7). While in the inner Lingdingyang Bay, the increased nutrient inputs only caused a slight change in Chl a content because the phytoplankton growth in this region was mostly light limited due to high water turbidity (Table 2). The concomitant changes in SOD and bottom DO were fairly small as well. Collectively, the high-nutrient scenario alone resulted in a 31% and 34% growth in the area affected by low oxygen (HA4) and hypoxia (HA3) relative to the 1990s, respectively (Table 3).

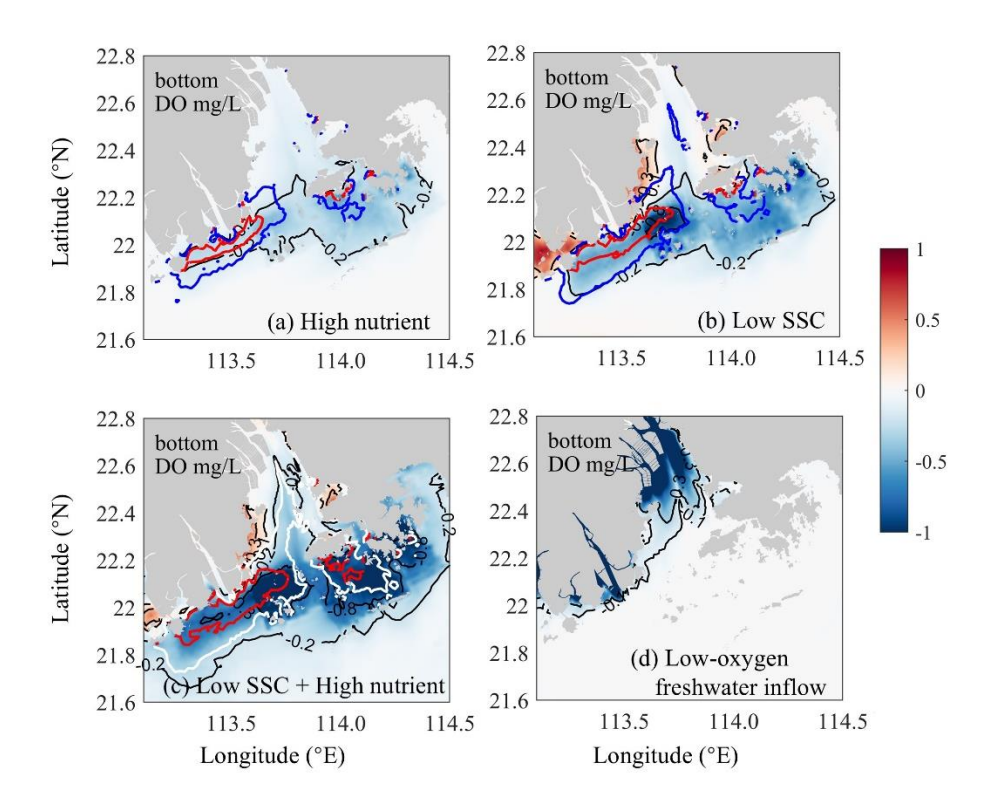


Fig. 6. Bottom DO changes induced by (a) riverine nutrient increases (the High-nutrient case minus the 1990s case), (b) riverine SSC declines (the Low-SSC case minus the 1990s case), (c) the combined effects of nutrient increases and SSC declines (the DO-restore case minus the 1990s case), and (d) riverine DO declines (the DO-restore case minus the 2010s case), respectively. The blue and white contour lines represent DO = 4 mg/L for the respective cases, and the red contour lines represent DO = 3 mg/L.

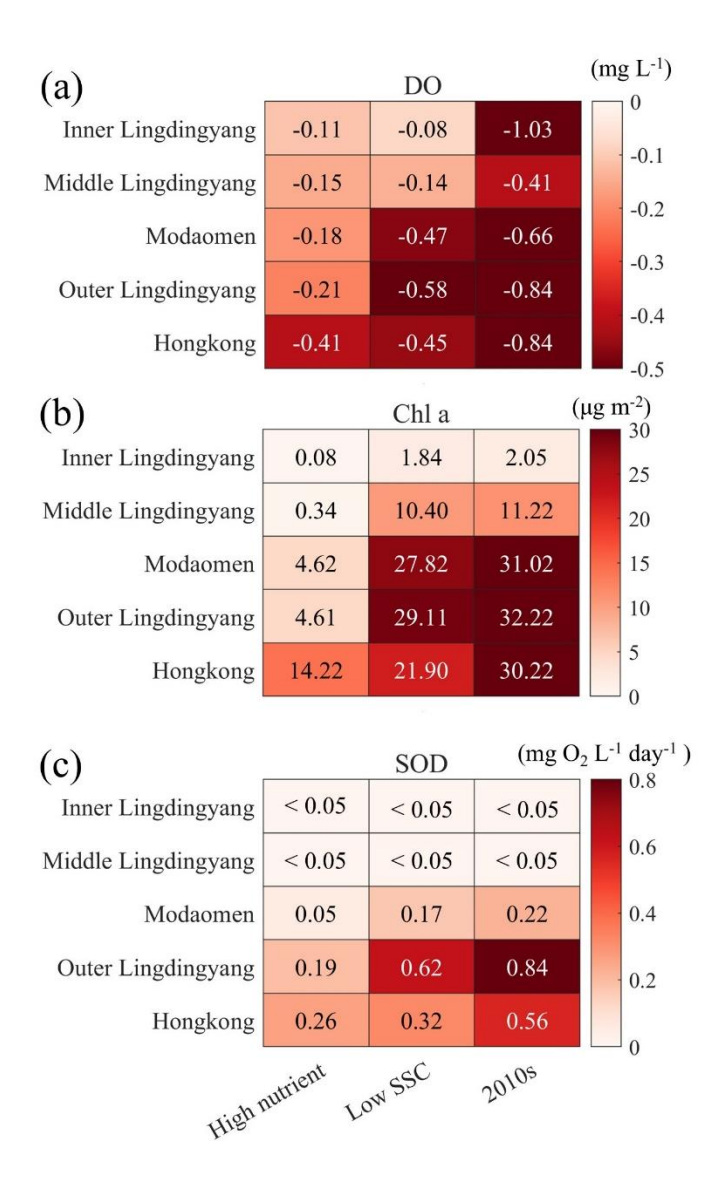


Fig. 7. Changes of (a) bottom DO concentration, (b) vertically-integrated Chl a content, and (c) SOD in subregions of the PRE for the High-nutrient, the Low-SSC, and the 2010s cases relative to the 1990s case.

Compared with the High-nutrient case, reducing the riverine suspended sediment loads from the 1990s to the 2020s-2010s alone (Low-SSC case) imposed a greater impact on the DO conditions, causing more extensive and intense deoxygenation through the PRE (Fig. 6b). Apparent DO decline (exceeding 0.3 mg/L relative to the 1990s) occurred within the lower PRE, similar to that of the changing riverine nutrients described above. This is also attributed to the intensified SOD (with an increment of 0.17-0.62 mg O₂ L⁻¹ day⁻¹, accounting for 57.1%-77.3% of the total increment during

the two periods; Fig. 7c), accompanied by a prominent increase in Chl a content (by 21.9-29.1 μg/m², accounting for 72.4%-90.3% of the total increment; Fig. 7b) due to the improved light condition (the relief of light limitation; Table 2). The SSC-induced changes in these biogeochemical factors were more pronounced in the outer Lingdingyang Bay and Modaomen sub-estuary than in other regions including the Hong Kong waters, which coincided with the alterations in deoxygenation among the subregions (Fig. 7). Overall, under the low-SSC scenario the low-oxygen area (HA4) and hypoxic area (HA3) expanded by 47% and 95% compared to the 1990s, respectively (Table 3). As shown in Figure 7 and Table 3, the combined effect of reducing SSC and increasing nutrient inputs (DO-restore case) led to a significant expansion of low-oxygen conditions, with hypoxic areas (HA4) and low-oxygen areas (HA3) reaching 2409.7 km² and 617.2 km², respectively. This combined effect exceeded the sum of changes induced by individual river inputs, highlighting the nonlinear interaction between SSC and nutrient loading. In regions such as Outer Lingdingyang and Hong Kong, the combined effect was amplified, while in regions such as Inner and Middle Lingdingyang, the combined effect was less than the sum of individual effects. The growth of phytoplankton is not a linear process in response to various influencing factors; instead, these factors interact cumulatively. Therefore, when different factors are combined, their combined effect can exceed the impact of individual factors acting alone.

573

574

575

576

577

578

579

580

581

582

583

584

585

586

587

588

589

590

591

592

593

594

595

596

597

598

599

600

With respect to the influence of altered riverine DO influx, it could be deduced from the difference between the 2010s and the DO-restore cases (Fig. 6d). There was a considerable DO decrease (by over 0.8 mg/L) in the bottom waters adjacent to the river outlets (also in the surface waters) owing to the low-oxygen inflows from the upstream river channels. The impact of these low-oxygen waters was largely restricted within the upper Lingdingyang Bay under the effects of air-sea reoxygenation and water-column mixing along with the river plume transport. Collectively, reducing the riverine DO content from the 1990s to the 2020s-2010s alone resulted in an enlargement of low-

oxygen area by nearly 515.8 km² (derived by subtracting the HA4 of the 2010s case from that of the DO-restore case; Table 3).

4. Discussion

601

602

603

604

605

606

607

608

609

610

611

612

613

614

615

616

617

618

619

620

621

622

623

624

625

626

4.1 Impacts of decadal changes in riverine inputs on deoxygenation off the PRE

By integrating long-term observations with physical-biogeochemical model

simulations, we revealed significant bottom-water deoxygenation in the Pearl River Estuary over the past three decades, driven by changes in riverine inputs. From the 1990s to 2020s2010s, summer inflows of DIN and DIP increased by ~100% and ~225%, while SSC decreased by ~60% due to human activities like dam construction (Liu et al., 2022) and reforestation (Cao et al., 2023). Concurrently, oxygen depletion from terrestrial pollutants reduced riverine DO concentrations by 46% (Ma et al., 2024). These shifts collectively intensified bottom-water low-oxygen conditions in PRE (Fig. 5), with model simulations showing a 148% expansion in summer low-oxygen areas (DO < 4 mg/L) and a 192% decrease increase in hypoxic areas (DO < 3 mg/L). Lowoxygen events also become more persistent, lasting longer (~15-35 days during June-August) and expanding vertically by $\sim 1-4$ m and (Table 3)(Fig 5.g-h). More interestingly, the PRE has developed three distinct hypoxic centers (including the inner Lingdingyang Bay, Modaomen sub-estuary, and Hong Kong waters) controlled by different dominant factors, which renders the deoxygenation problem in this region as a great reference for estuaries and coastal systems worldwide. Specifically, the impact of riverine low-oxygen waters was confined within the upper estuary close to the river outlets, leading to a ~44% increase in the low-oxygen area relative to the 1990s. Such local low-oxygen issue could be mitigated to a large extent if the riverine DO recovered to a comparatively higher level (e.g., ~6.5 mg/L in the 1990s) according to the DO-restore scenario (Fig. 6d). Reduced water turbidity downstream facilitates

the upstream transport of nutrients, promoting eutrophication and oxygen depletion in the lower reaches, which is highly sensitive to changes in riverine nutrient and sediment inputs. As indicated in the High-nutrient and the Low-SSC cases, the increased nutrient inputs and declined suspended sediment loads have separately alleviated the nutrient and light limitations on algae growth in the region, thereby stimulating phytoplankton blooms and local production of organic matter to support subsurface oxygen consumption (dominated by sediment oxygen uptake, SOD; Fig. 7).

While previous studies have primarily examined the impacts of riverine inputs of freshwater, nutrients and organic matter, this study provides a comprehensive investigation of how suspended sediment reduction influences estuarine dissolved oxygen dynamics. In the PRE, the riverine SSC reduction played a more important role in driving the long-term low-oxygen expansion than nutrient increase. Its synergistic effect with the riverine nutrient changes could further amplify the exacerbation of eutrophication and subsequent deoxygenation, resulting in an enlarged growth in the low-oxygen area (by 104%) and hypoxic area (by 192%) that was notably larger than the total of their partial contributions (Table 3), and reached 70% of the total impact from combined SSC, nutrient, and low-oxygen changes (148% low-oxygen expansion).

It is worth mentioning that the relative importance of the riverine nutrient and SSC changes were different between the two hypoxic centers in the lower PRE, depending upon their distances and water flow conditions from the river outlets. Closer to the river outlets, the Modaomen sub-estuary and its surrounding waters (located on the western side of the coastal transition zone off the PRE) possessed a fairly high SSC level, which imposed a stronger light limitation on the growth of phytoplankton in the region, ultimately making the oxygen dynamics more susceptible to the decline in riverine SSC. This non-additive characteristic— underscores the need for integrated management approaches that simultaneously address both nutrient loads and suspended sediment-mediated light conditions indicates that considering either nutrients or light alone in estuarine management is not sufficiently comprehensive.

Suspended sediments were confined to the coastal area of Modaomen by water currents (Fig. 1b), resulting in a significant decrease in sediment deposition in this region, which greatly improved light availability, ultimately making the oxygen dynamics more susceptible to the decline in riverine SSC. On the contrary, the Hong Kong waters and adjacent coastal areas (located on the eastern side of the coastal transition zone) far from the river outlets were less affected by the riverine inputs, where the relatively low nutrient levels promoted more sensitive responses of biogeochemical processes (e.g. primary production and SOD) and hypoxia occurrences to nutrient variations. Besides, the complex island topography near Hong Kong (Fig. 1b) creates hydrodynamic barriers that restrict the offshore transport of suspended sediments.

4.2 Nutrient control and hypoxia mitigation in the context of sediment declines

Our results <u>highlight underscored</u> the substantial spatial variability in <u>how the</u> regulation of riverine inputs <u>influence on-deoxygenation</u>, <u>emphasizing highlighting</u> the need for more refined and targeted <u>strategies to mitigate strategies for hypoxia mitigation</u>. While the effects of Compared with the riverine nutrients on hypoxia have been widely studied, the role regulatory effects of SSC in modulating on eutrophication and hypoxia have has received comparatively less attention. This is particularly relevant in systems like the PRE, which has experienced a dramatic 60% decline in sediment since the 1980s due to dam construction and land-use changes.

In the PRE, our model simulations demonstrate that SSC-mediated light limitation critically influences deoxygenation dynamics. When SSC declines are omitted, model simulations overestimate nutrient-driven productivity and underestimate hypoxia expansion. This oversight-suggests that for systems experiencing pronounced sediment reductions, overlooking SSC effects previous studies may have overestimated nutrient impacts when failing to account for SSC-mediated processes required to align model simulations with observed deoxygenation patterns. Such model overcompensation

could lead to <u>overlypotentially</u> optimistic assessments of <u>hypoxia mitigation</u> <u>effectiveness under proposed</u>-nutrient control <u>efficacyplans</u>. It is therefore critical to disentangle <u>and quantitatively re-evaluate</u> the relative contributions of riverine nutrients versus SSC changes to coastal deoxygenation <u>trenddynamics over recent decades</u>. As demonstrated in the PRE <u>case study</u>, the current low-SSC <u>environmentregime</u> suggests <u>that</u> more stringent nutrient reductions <u>than previously estimated</u> might be required to effectively curb deoxygenation <u>compared to conditions with higher SSC</u>.

Furthermore, it should be noted that a Although the dam constructions in the Pearl River Basin, have mostly completed beforesince the 2000s, have driven significant declines in SSC, the future it is still unclear whether the declining trends of riverine SSC remain uncertainwill persist in the future. For instance, recent the reforestation efforts have in recent years has shown to be effectively in reduceding the summer freshwater discharges and sediment loads in the Pearl River Basin (Cao et al., 2023). This evolving situation context underscores that changes in SSC variations will continue to shape play a defining role in future oxygen dynamics, introducing compounding uncertainties for hypoxia mitigation strategies.

Similar relationship between SSC and eutrophication or hypoxia have been observed in other systems facing rapid anthropogenic changes. Notably, analogous sediment oxygen coupling mechanisms are emerging in other hypoxic systems. For example, the Yangtze River Estuary has seen ait was reported that the decrease of riverine SSC (by ~56% decrease in SSC over the past decades, which has been linked to) appeared to be the predominant factor for the intensifying eutrophication (with a 61% increase in the Chl a concentration, indicating intensified eutrophication) in the Yangtze River Estuary over the past decades (Wang et al., 2019). In addition, several modelling studies have showed shown that the dam constructions in the upper regions of the Guadiana Estuary have led tosignificantly reduced the water turbidity and exacerbated eutrophication in the lower estuary (Domingues et al., 2012; Barbosa et al., 2010). A global-scale survey revealed that the sediment loads in 414 major rivers has have

approximately decreased by approximately 51% since the 2000s due to human activities (Dethier et al., 2022). This trend highlights the need for further investigation into how sediment declines impact eutrophication and deoxygenation on a global scale. Suggesting that the deteriorating eutrophication and deoxygenation in the context of sediment declines has become a global concern and merits more attention and investigations in the future.

It is also important to recognize that While our study emphasizes the impacts of reduced suspended sediments, human activities may can conversely increase sediment loads in estuaries. For example, land-use changes such as deforestation_(Kasai et al., 2005) or and industrialization (Syvitski and Kettner, 2011) may can exacerbate soil erosion and sediment transport, leading to higher suspended sediment concentrations in the water. In such cases, light attenuation due to increased turbidity may suppress phytoplankton growth and reduce primary production, potentiallythereby mitigating hypoxia. Therefore, the effects of SSC are system-specific and depend on the direction and magnitude of sediment trends.

Some caveats <u>into</u> our work require further <u>investigationstudies</u>. First, our light attenuation parameterization <u>is based onbuilds upon</u> the empirical formulation of Ditoro (2001), <u>which has beenpreviously</u> validated for the <u>Pearl River Estuary</u> (PRE) through biogeochemical consistency checks (Wang et al., 2018). While this approach successfully captured observed oxygen dynamics in our simulations,—<u>it explicitly resolves only the chlorophyll and suspended sediment effects on light attenuation two key simplifications require explicit discussion. The current light attenuation parameterization in our model primarily accounts for the effects of chlorophyll and <u>suspended sediments</u>. Previous studies have <u>showndemonstrated</u> that <u>CDOM</u> (colored dissolved organic matter <u>(CDOM)</u> also plays a significant role in light attenuation within the PRE (Cao et al., 2003; Wang et al., 2010), particularly during algal bloom periods. <u>The model's calibration to observed biogeochemical variables may partially compensate for CDOM's influence</u>, but future work should explicitly parameterize</u>

CDOM's optical properties through both modeling refinements and sustained monitoring to better quantify its role in oxygen dynamics. Although our model does not explicitly treat CDOM as an independent variable, its influence is indirectly accounted for within the existing parameterization. However, to accurately quantify CDOM's contribution to oxygen dynamics including its long-term trends future work should incorporate an explicit representation of CDOM's effects on light attenuation in the model, alongside sustained observational monitoring of CDOM. In addition to Apart from anthropogenic influences activities, changes alterations in regional physical conditions due toaligning with climate change, s such as wind speed and freshwater discharge, could also affectregulate the long-term deoxygenation trends in coastal regions (Yu et al., 2015; Chen et al., 2024). Besides, tThe impacts of ocean warming on deoxygenation (Laurent et al., 2018) remain unclear in the PRE despite evidence of as well, although warming has already been observed in the PRE (Cheung et al., 2021). Its The compounding factors of warming such as sea-level rise (Hong et al., 2020) may introduce additional further complexity to hypoxia dynamicsevolution through cascading ecosystem effects. While these factors werehave not been considered in this study, understanding -the interplay between relative contributions of human activities and climate changes is crucials represent a significant topic for future research oninvestigations, which can facilitate a more comprehensive understanding of oxygen dynamics and hypoxia development in estuaries and coastal systems.

5. Conclusion

738

739

740

741

742

743

744

745

746

747

748

749

750

751

752

753

754

755

756

757

758

759

760

761

762

763

764

We applied a well-validated physical-biogeochemical model to reconstruct the summertime oxygen distributions in the PRE during two representative periods (the 1990s and the 2010s) and to disentangle the contribution of alterations in riverine inputs (i.e., suspended sediments, nutrients, and oxygen concentration) to the long-term deoxygenation off the PRE based on a suite of model experiments. We found that owing to the changes of riverine inputs over the past three decades, the low-oxygen and

hypoxic areas in the bottom waters of the PRE have expanded by about 1.5 times and two-fold, respectively, with the duration time prolonged by ~15-35 days in summer. Concurrently, three hypoxic centers dominated by distinct factors were identified. Single-factor experiments suggested that a 46% decrease in riverine DO alone expanded low-oxygen areas by ~44% in the upper PRE, a 60% SSC reduction alone caused a 47% expansion in the lower PRE, and nutrient increases alone (100% DIN, 225% phosphate) drove a 31% expansion. Scenario simulations revealed that the decline in riverine oxygen concentration has caused a low-oxygen expansion (by ~44%) in the upper PRE. By comparison, the alterations in riverine nutrients and suspended sediments have separately provided better nutrient and light conditions to promote higher production of labile organic matter, which jointly maintained considerable oxygen depletions and exacerbated the low-oxygen conditions in the lower PRE. The relative importance of the changing riverine nutrients and suspended sediments to deoxygenation varied between subregions. The suspended sediment reduction was the predominated factor in the downstream regions close to the river outlets (e.g. the Modaomen sub-estuary), while the nutrient increase exerted a more substantial influence in the regions far from the river outlets (e.g. the Hong Kong waters). Our study demonstrates that highlights the significant role of the declined suspended sediments have significantly exacerbated in the low-oxygen conditionsexpansion off the PRE, with effects that synergistically intensify when combined with increasing nutrient loadswhich can further amplify the effect in association with the increasing nutrients. These findings highlight the need for dual-control strategies addressing both nutrient inputs and sediment-mediated light availability in coastal management. Give the global declines in riverine suspended sediments, we emphasize that effective hypoxia mitigation requires integrated approaches accounting for these interacting drivers. Therefore, in _the context of global regimes changes of riverine suspended sediments, we call for an urgent re-evaluation of the impacts of riverine inputs on deoxygenation in addition to nutrients in order to better understand the mechanism

765

766

767

768

769

770

771

772

773

774

775

776

777

778

779

780

781

782

783

784

785

786

787

788

789

790

791

793	controlling hypoxia and thereby proposing effective mitigation strategies.
794	
795	CRediT authorship contribution statement
796	Yue-Nan: Investigation, Model experiments, Formal analysis, Visualization,
797	Writing-original draft. Zheng-Chen: Model experiments, Writing-review. Bin-Wang:
798	Writing-review. Bo-Liang: Writing-review. Jiatang-Hu: Project administration,
799	Supervision, Conceptualization, Writing-review & editing.
800	Declaration of competing interest
801	The authors declare that they have no known competing financial interests or
802	personal relationships that could have appeared to influence the work reported in this
803	paper.
804	Acknowledgements
805	This work was supported by a grant from the Southern Marine Science and
806	Engineering Guangdong Laboratory (Zhuhai) (Project. SML2023SP220) and two
807	consulting projects (ZB-2023-005, ZB-2023-054) to JH. This work was supported by
808	the National Natural Science Foundation of Guangdong Province (grant no.
809	2025A1515010991) and a grant from the Southern Marine Science and Engineering
810	Guangdong Laboratory (Zhuhai) (Project. SML2024SP024) to JH, and the National
811	Natural Science Foundation of China (grand no. 42206141) to LB.
812	
813	Data availability
814	The dissolved oxygen observation datasets off the Pearl River Estuary were
815	obtained from published studies (Hu et al., 2021, DOI: 10.5194/bg-18-5247-2021; Su
816 817	et al., 2017, DOI: 10.5194/bg-14-4085-2017; Li et al., 2021, DOI: 10.1029/2020JC016700; Chen et al., 2020, DOI: 10.1029/2019JG005596) and the
818	Hong Kong Environmental Protection Department

819	(lettray/od ania and asychle/EDICDIVED/maning/yyyyyy and asychle). The absorption
019	(<u>https://cd.epic.epd.gov.hk/EPICRIVER/marine/www.epd.gov.hk</u>). The observed
820	nutrients, oxygen, and suspended sediments data in the Pearl River are available from
821	Hu et al. (2021) and publicly accessible databases maintained by China's Ministry of
822	Ecology and Environment (https://www.mee.gov.cn/) Department of Ecology and
823	Environment of Guangdong Province (https://gdee.gd.gov.cn/hjjce/jahy/index.html)
824	and the China River Sediment Bulletin (http://www.mwr.gov.cn/sj/tjgb/zghlnsgb/).
825	

826 Reference

- Barbosa, A. B., Domingues, R. B., and Galvão, H. M.: Environmental Forcing of
- 828 Phytoplankton in a Mediterranean Estuary (Guadiana Estuary, South-western Iberia):
- A Decadal Study of Anthropogenic and Climatic Influences, Estuaries and Coasts, 33,
- 830 324-341, https://doi.org/10.1007/s12237-009-9200-x, 2010.
- Bianchi, T. S., DiMarco, S. F., Cowan, J. H., Hetland, R. D., Chapman, P., Day, J. W.,
- and Allison, M. A.: The science of hypoxia in the Northern Gulf of Mexico: A review,
- 833 Science of The Total Environment, 408, 1471-1484,
- 834 https://doi.org/10.1016/j.scitotenv.2009.11.047, 2010.
- Breitburg, D., Levin, L. A., Oschlies, A., Grégoire, M., Chavez, F. P., Conley, D. J.,
- 836 Garçon, V., Gilbert, D., Gutiérrez, D., Isensee, K., Jacinto, G. S., Limburg, K. E.,
- Montes, I., Naqvi, S. W. A., Pitcher, G. C., Rabalais, N. N., Roman, M. R., Rose, K. A.,
- 838 Seibel, B. A., Telszewski, M., Yasuhara, M., and Zhang, J.: Declining oxygen in the
- 839 global ocean and coastal waters, Science, 359, eaam7240,
- 840 https://doi.org/10.1126/science.aam7240, 2018.
- 841 Bussi, G., Darby, S. E., Whitehead, P. G., Jin, L., Dadson, S. J., Voepel, H. E.,
- Vasilopoulos, G., Hackney, C. R., Hutton, C., Berchoux, T., Parsons, D. R., and
- Nicholas, A.: Impact of dams and climate change on suspended sediment flux to the
- 844 Mekong delta, Science of The Total Environment, 755, 142468,
- 845 https://doi.org/10.1016/j.scitotenv.2020.142468, 2021.
- 846 Cao, W., Yang, Y., Xu, X., Huang, L., and Zhang, J.: Regional patterns of particulate
- spectral absorption in the Pearl River estuary, Chinese Science Bulletin, 48, 2344-2351,
- 848 https://doi.org/10.1360/03wd0151, 2003.
- 849 Cao, Z., Duan, H., Ma, R., Shen, M., and Yang, H.: Remarkable effects of greening
- 850 watershed on reducing suspended sediment flux in China's major rivers, Science
- 851 Bulletin, 68, 2285-2288, https://doi.org/10.1016/j.scib.2023.08.036, 2023.
- Carstensen, J., Andersen, J. H., Gustafsson, B. G., and Conley, D. J.: Deoxygenation of
- the Baltic Sea during the last century, Proceedings of the National Academy of Sciences
- 854 of the United States of America, 111, 5628-5633,
- https://doi.org/10.1073/pnas.1323156111, 2014.
- 856 Chen, J. Y., Pan, D. L., Liu, M. L., Mao, Z. H., Zhu, O. K., Chen, N. H., Zhang, X. Y.,
- 857 and Tao, B. Y.: Relationships Between Long-Term Trend of Satellite-Derived
- 858 Chlorophyll-a and Hypoxia Off the Changjiang Estuary, ESTUARIES AND COASTS,
- 40, 1055-1065, https://doi.org/10.1007/s12237-016-0203-0, 2017.
- 860 Chen, L., Zhang, X., He, B., Liu, J., Lu, Y., Liu, H., Dai, M., Gan, J., and Kao, S.-J.:
- Dark Ammonium Transformations in the Pearl River Estuary During Summer, Journal
- 862 of Geophysical Research: Biogeosciences, 125, e2019JG005596,
- 863 https://doi.org/10.1029/2019JG005596, 2020.
- 864 Chen, Z., Yu, L., and Hu, J.: Disentangling the contributions of anthropogenic nutrient
- solution input and physical forcing to long-term deoxygenation off the Pearl River Estuary,
- 866 China, Water Research, 265, 122258, https://doi.org/10.1016/j.watres.2024.122258,

- 867 2024.
- 868 Cheung, Y. Y., Cheung, S., Mak, J., Liu, K., Xia, X., Zhang, X., Yung, Y., and Liu, H.:
- 869 Distinct interaction effects of warming and anthropogenic input on diatoms and
- dinoflagellates in an urbanized estuarine ecosystem, Global Change Biology, 27, 3463-
- 871 3473, https://doi.org/10.1111/gcb.15667, 2021.
- 872 Cormier, J. M., Coffin, M. R. S., Pater, C. C., Knysh, K. M., Gilmour, R. F., Guyondet,
- 873 T., Courtenay, S. C., and van den Heuvel, M. R.: Internal nutrients dominate load and
- drive hypoxia in a eutrophic estuary, Environmental Monitoring and Assessment, 195,
- 875 1211, https://doi.org/10.1007/s10661-023-11621-y, 2023.
- 876 Cullen, J. J.: Subsurface Chlorophyll Maximum Layers: Enduring Enigma or Mystery
- 877 Solved?, in: ANNUAL REVIEW OF MARINE SCIENCE, VOL 7, edited by: Carlson,
- 878 C. A., and Giovannoni, S. J., 207-239, 10.1146/annurev-marine-010213-135111, 2015.
- 879 Dethier, E. N., Renshaw, C. E., and Magilligan, F. J.: Rapid changes to global river
- 880 suspended sediment flux by humans, Science, 376, 1447-1452,
- 881 https://doi.org/10.1126/science.abn7980, 2022.
- 882 Diaz, R. J. and Rosenberg, R.: Spreading dead zones and consequences for marine
- 883 ecosystems, Science, 321, 926-929, https://doi.org/10.1126/science.1156401, 2008.
- 884 DiToro, D. M.: Sediment flux modeling, John Wiley & Sons, 656 pp., ISBN
- 885 9780471135357, 2001.
- Domingues, R. B., Barbosa, A. B., Sommer, U., and Galvão, H. M.: Phytoplankton
- composition, growth and production in the Guadiana estuary (SW Iberia): Unraveling
- changes induced after dam construction, Science of The Total Environment, 416, 300-
- 313, https://doi.org/10.1016/j.scitotenv.2011.11.043, 2012.
- 890 Ge, J., Torres, R., Chen, C., Liu, J., Xu, Y., Bellerby, R., Shen, F., Bruggeman, J., and
- 891 Ding, P.: Influence of suspended sediment front on nutrients and phytoplankton
- 892 dynamics off the Changjiang Estuary: A FVCOM-ERSEM coupled model experiment,
- 893 Journal of Marine Systems, 204, 103292,
- 894 https://doi.org/10.1016/j.jmarsys.2019.103292, 2020.
- Hagy, J. D., Boynton, W. R., and Jasinski, D. A.: Modelling phytoplankton deposition
- 896 to Chesapeake Bay sediments during winter-spring: interannual variability in relation
- 897 to river flow, ESTUARINE COASTAL AND SHELF SCIENCE, 62, 25-40,
- 898 https://doi.org/10.1016/j.ecss.2004.08.004, 2005.
- Hong, B., Liu, Z., Shen, J., Wu, H., Gong, W., Xu, H., and Wang, D.: Potential physical
- 900 impacts of sea-level rise on the Pearl River Estuary, China, Journal of Marine Systems,
- 901 201, 103245, https://doi.org/10.1016/j.jmarsys.2019.103245, 2020.
- Howarth, R., Chan, F., Conley, D. J., Garnier, J., Doney, S. C., Marino, R., and Billen,
- 903 G.: Coupled biogeochemical cycles: eutrophication and hypoxia in temperate estuaries
- and coastal marine ecosystems, Frontiers in Ecology and the Environment, 9, 18-26,
- 905 https://doi.org/10.1890/100008, 2011.
- Hu, J. and Li, S.: Modeling the mass fluxes and transformations of nutrients in the Pearl
- 907 River Delta, China, Journal of Marine Systems, 78, 146-167,
- 908 https://doi.org/10.1016/j.jmarsys.2009.05.001, 2009.

- 909 Hu, J., Li, S., and Geng, B.: Modeling the mass flux budgets of water and suspended
- 910 sediments for the river network and estuary in the Pearl River Delta, China, Journal of
- 911 Marine Systems, 88, 252-266, https://doi.org/10.1016/j.jmarsys.2011.05.002, 2011.
- 912 Hu, J., Zhang, Z., Wang, B., and Huang, J.: Long-term spatiotemporal variations in and
- expansion of low-oxygen conditions in the Pearl River estuary: a study synthesizing
- 914 observations during 1976–2017, Biogeosciences, 18, 5247-5264,
- 915 https://doi.org/10.5194/bg-18-5247-2021, 2021.
- 916 Huang, Y.-G., Yang, H.-F., Jia, J.-J., Li, P., Zhang, W.-X., Wang, Y. P., Ding, Y.-F., Dai,
- 917 Z.-J., Shi, B.-W., and Yang, S.-L.: Declines in suspended sediment concentration and
- 918 their geomorphological and biological impacts in the Yangtze River Estuary and
- 919 adjacent sea, Estuarine, Coastal and Shelf Science, 265, 107708,
- 920 https://doi.org/10.1016/j.ecss.2021.107708, 2022.
- 921 HydroQual, Inc.: User's Guide for RCA (Release 3.0), HydroQual, Inc., Mahwah, NJ,
- 922 2004.
- 923 Kasai, M., Brierley, G. J., Page, M. J., Marutani, T., and Trustrum, N. A.: Impacts of
- 924 land use change on patterns of sediment flux in Weraamaia catchment, New Zealand,
- 925 CATENA, 64, 27-60, https://doi.org/10.1016/j.catena.2005.06.014, 2005.
- Lai, Y., Jia, Z., Xie, Z., Li, S., and Hu, J.: Water quality changes and shift in mechanisms
- 927 controlling hypoxia in response to pollutant load reductions: A case study for Shiziyang
- 928 Bay, Southern China, Science of The Total Environment, 842, 156774,
- 929 https://doi.org/10.1016/j.scitotenv.2022.156774, 2022.
- 930 Laurent, A., Fennel, K., Ko, D. S., and Lehrter, J.: Climate change projected to
- exacerbate impacts of coastal eutrophication in the northern Gulf of Mexico, Journal of
- 932 Geophysical Research: Oceans, 123, 3408-3426,
- 933 https://doi.org/10.1002/2017JC013583, 2018.
- Lee, Z.-P., Du, K.-P., and Arnone, R.: A model for the diffuse attenuation coefficient of
- 935 downwelling irradiance, Journal of Geophysical Research: Oceans, 110,
- 936 https://doi.org/10.1029/2004JC002275, 2005.
- Li, D., Gan, J., Hui, C., Yu, L., Liu, Z., Lu, Z., Kao, S.-j., and Dai, M.: Spatiotemporal
- 938 Development and Dissipation of Hypoxia Induced by Variable Wind-Driven Shelf
- 939 Circulation off the Pearl River Estuary: Observational and Modeling Studies, Journal
- 940 of Geophysical Research: Oceans, 126, e2020JC016700,
- 941 https://doi.org/10.1029/2020JC016700, 2021.
- 942 Li, G., Liu, J., Diao, Z., Jiang, X., Li, J., Ke, Z., Shen, P., Ren, L., Huang, L., and Tan,
- 943 Y.: Subsurface low dissolved oxygen occurred at fresh- and saline-water intersection of
- 944 the Pearl River estuary during the summer period, Marine Pollution Bulletin, 126, 585-
- 945 591, https://doi.org/10.1016/j.marpolbul.2017.09.061, 2018.
- 946 Li, X., Lu, C., Zhang, Y., Zhao, H., Wang, J., Liu, H., and Yin, K.: Low dissolved
- 947 oxygen in the Pearl River estuary in summer: Long-term spatio-temporal patterns,
- 948 trends, and regulating factors, Marine Pollution Bulletin, 151, 110814,
- 949 https://doi.org/10.1016/j.marpolbul.2019.110814, 2020.
- 950 Liu, Z., Fagherazzi, S., Liu, X., Shao, D., Miao, C., Cai, Y., Hou, C., Liu, Y., Li, X., and

- 951 Cui, B.: Long-term variations in water discharge and sediment load of the Pearl River
- 952 Estuary: Implications for sustainable development of the Greater Bay Area, Frontiers
- 953 in Marine Science, 9, 983517, https://doi.org/10.3389/fmars.2022.983517, 2022.
- 954 Lu, Z., Gan, J., Dai, M., Liu, H., and Zhao, X.: Joint Effects of Extrinsic Biophysical
- 955 Fluxes and Intrinsic Hydrodynamics on the Formation of Hypoxia West off the Pearl
- 956 River Estuary, Journal of Geophysical Research: Oceans, 123, 6241-6259,
- 957 https://doi.org/10.1029/2018jc014199, 2018.
- 958 Luo, X., Yang, Q., and Jia, L.: The Riverbed Evolution of the River-Network System
- 959 in the Pearl River Delta, Sun Yat-sen University Press, Guangzhou, China, 2002.
- 960 Ma, C., Zhao, J., Ai, B., Sun, S., and Yang, Z.: Machine Learning Based Long-Term
- 961 Water Quality in the Turbid Pearl River Estuary, China, Journal of Geophysical
- 962 Research: Oceans, 127, e2021JC018017, https://doi.org/10.1029/2021JC018017, 2022.
- Ma, R., Chen, Z., Wang, B., Xu, C., Jia, Z., Li, L., and Hu, J.: Spatiotemporal variations
- and controlling mechanism of low dissolved oxygen in a highly urbanized complex
- 965 river system, Journal of Hydrology: Regional Studies, 52, 101691,
- 966 https://doi.org/10.1016/j.ejrh.2024.101691, 2024.
- 967 Murphy, R. R., Kemp, W. M., and Ball, W. P.: Long-Term Trends in Chesapeake Bay
- 968 Seasonal Hypoxia, Stratification, and Nutrient Loading, ESTUARIES AND COASTS,
- 969 34, 1293-1309, https://doi.org/10.1007/s12237-011-9413-7, 2011.
- 970 Pitcher, G. C., Aguirre-Velarde, A., Breitburg, D., Cardich, J., Carstensen, J., Conley,
- 971 D. J., Dewitte, B., Engel, A., Espinoza-Morriberón, D., Flores, G., Garçon, V., Graco,
- 972 M., Grégoire, M., Gutiérrez, D., Hernandez-Ayon, J. M., Huang, H.-H. M., Isensee, K.,
- 973 Jacinto, M. E., Levin, L., Lorenzo, A., Machu, E., Merma, L., Montes, I., Swa, N.,
- 974 Paulmier, A., Roman, M., Rose, K., Hood, R., Rabalais, N. N., Salvanes, A. G. V.,
- 975 Salvatteci, R., Sánchez, S., Sifeddine, A., Tall, A. W., Plas, A. K. v. d., Yasuhara, M.,
- 276 Zhang, J., and Zhu, Z. Y.: System controls of coastal and open ocean oxygen depletion,
- 977 Progress in Oceanography, 197, 102613, https://doi.org/10.1016/j.pocean.2021.102613,
- 978 2021.
- Roman, M. R., Brandt, S. B., Houde, E. D., and Pierson, J. J.: Interactive effects of
- 980 Hypoxia and temperature on coastal pelagic zooplankton and fish, Frontiers in Marine
- 981 Science, 6, https://doi.org/10.3389/fmars.2019.00139, 2019.
- 982 Su, J., Dai, M., He, B., Wang, L., Gan, J., Guo, X., Zhao, H., and Yu, F.: Tracing the
- origin of the oxygen-consuming organic matter in the hypoxic zone in a large eutrophic
- 984 estuary: the lower reach of the Pearl River Estuary, China, Biogeosciences, 14, 4085-
- 985 4099, https://doi.org/10.5194/bg-14-4085-2017, 2017.
- 986 Syvitski, J. P. M. and Kettner, A.: Sediment flux and the Anthropocene, Philosophical
- 987 Transactions of the Royal Society A: Mathematical, Physical and Engineering Sciences,
- 988 369, 957-975, https://doi.org/10.1098/rsta.2010.0329, 2011.
- Wang, B., Hu, J., Li, S., and Liu, D.: A numerical analysis of biogeochemical controls
- 990 with physical modulation on hypoxia during summer in the Pearl River estuary,
- 991 Biogeosciences, 14, 2979-2999, https://doi.org/10.5194/bg-14-2979-2017, 2017.
- Wang, B., Hu, J., Li, S., Yu, L., and Huang, J.: Impacts of anthropogenic inputs on

- 993 hypoxia and oxygen dynamics in the Pearl River estuary, Biogeosciences, 15, 6105-
- 994 6125, https://doi.org/10.5194/bg-15-6105-2018, 2018.
- 995 Wang, G., Cao, W., Yang, Y., Zhou, W., Liu, S., and Yang, D.: Variations in light
- absorption properties during a phytoplankton bloom in the Pearl River estuary,
- 997 Continental Shelf Research, 30, 1085-1094,
- 998 https://doi.org/10.1016/j.envres.2021.111579, 2010.
- 999 Wang, H., Dai, M., Liu, J., Kao, S.-J., Zhang, C., Cai, W.-J., Wang, G., Qian, W., Zhao,
- 1000 M., and Sun, Z.: Eutrophication-Driven Hypoxia in the East China Sea off the
- 1001 Changjiang Estuary, Environmental Science & Technology, 50, 2255-2263,
- 1002 https://doi.org/10.1021/acs.est.5b06211, 2016.
- Wang, J. J., Bouwman, A. F., Liu, X. C., Beusen, A. H. W., Van Dingenen, R., Dentener,
- 1004 F., Yao, Y. L., Glibert, P. M., Ran, X. B., Yao, Q. Z., Xu, B. C., Yu, R. C., Middelburg,
- J. J., and Yu, Z. G.: Harmful Algal Blooms in Chinese Coastal Waters Will Persist Due
- 1006 to Perturbed Nutrient Ratios, ENVIRONMENTAL SCIENCE & TECHNOLOGY
- 1007 LETTERS, 8, 276-284, https://doi.org/10.1021/acs.estlett.1c00012, 2021.
- 1008 Wang, K., Chen, J., Jin, H., Li, H., Gao, S., Xu, J., Lu, Y., Huang, D., Hao, Q., and
- 1009 Weng, H.: Summer nutrient dynamics and biological carbon uptake rate in the
- 1010 Changjiang River plume inferred using a three end-member mixing model, Continental
- 1011 Shelf Research, 91, 192-200, https://doi.org/10.1016/j.csr.2014.09.013, 2014.
- Wang, Y., Wu, H., Lin, J., Zhu, J., Zhang, W., and Li, C.: Phytoplankton Blooms off a
- High Turbidity Estuary: A Case Study in the Changjiang River Estuary, Journal of
- 1014 Geophysical Research: Oceans, 124, 8036-8059, https://doi.org/10.1029/2019jc015343,
- 1015 2019.

- 1016 Wen, G., Liang, Z., Xu, X., Cao, R., Wan, Q., Ji, G., Lin, W., Wang, J., Yang, J., and
- Huang, T.: Inactivation of fungal spores in water using ozone: Kinetics, influencing
- 1018 factors and mechanisms, Water Research, 185, 116218,
- 1019 https://doi.org/10.1016/j.watres.2020.116218, 2020.
- Wu, C. S., Yang, S., Huang, S., and Mu, J.: Delta changes in the Pearl River estuary and
- its response to human activities (1954–2008), Quaternary International, 392, 147-154,
- 1022 https://doi.org/10.1016/j.quaint.2015.04.009, 2016.
- Yang, H., Wang, T., Yang, D., Yan, Z., Wu, J., and Lei, H.: Runoff and sediment effect
- of the soil-water conservation measures in a typical river basin of the Loess Plateau.
- 1025 CATENA, 243, 108218, https://doi.org/10.1016/j.catena.2024.108218, 2024.
- 1026 Yu, L., Gan, J., 2022. Reversing impact of phytoplankton phosphorus limitation on
- 1027 coastal hypoxia due to interacting changes in surface production and shoreward bottom
- oxygen influx. Water Res. 118094 https://doi.org/10.1016/j. watres.2022.118094.
- Yu, L., Fennel, K., Laurent, A., 2015. A modeling study of physical controls on hypoxia
- generation in the northern Gulf of Mexico. J. Geophys. Res. Oceans 120, 5019–5039.
- 1031 https://doi.org/10.1002/2014JC010634.
- Yu, L., Gan, J., Dai, M., Hui, C., Lu, Z., Li, D., 2020. Modeling the role of riverine
- organic matter in hypoxia formation within the coastal transition zone off the Pearl
- 1034 River Estuary. Limnol. Oceanogr. 9999, 1–17. https://doi.org/10.1002/lno.11616

- Zhang, S., Lu, X. X., Higgitt, D. L., Chen, C.-T. A., Han, J., and Sun, H.: Recent
- 1036 changes of water discharge and sediment load in the Zhujiang (Pearl River) Basin,
- 1037 China, Global and Planetary Change, 60, 365-380,
- 1038 https://doi.org/10.1016/j.gloplacha.2007.04.003, 2008.
- Zhang, Z., Wang, B., Li, S., Huang, J., and Hu, J.: On the Intra-annual Variation of
- 1040 Dissolved Oxygen Dynamics and Hypoxia Development in the Pearl River Estuary,
- 1041 Estuaries and Coasts, 45, 1305-1323, https://doi.org/10.1007/s12237-021-01022-0,
- 1042 2022.